

DOKUZ EYLÜL UNIVERSITY
GRADUATE SCHOOL OF NATURAL AND APPLIED SCIENCES

**VIBRO-ACOUSTIC ANALYSIS OF UNCERTAIN
COMPOSITE STRUCTURES USING
EXPERIMENTAL TECHNIQUES**



by
Altay OZANKAN

May, 2016
İZMİR

VIBRO-ACOUSTIC ANALYSIS OF UNCERTAIN COMPOSITE STRUCTURES USING EXPERIMENTAL TECHNIQUES

**A Thesis Submitted to the
Graduate School of Natural and Applied Sciences of Dokuz Eylül University
In Partial Fulfillment of the Requirements for the Degree of Master of Science
in Mechanical Engineering, Machine Theory and Dynamics Program**

**by
Altay OZANKAN**

**May, 2016
İZMİR**

M.Sc. THESIS EXAMINATION RESULT FORM

We have read the thesis entitled “**VIBRO-ACOUSTIC ANALYSIS OF UNCERTAIN COMPOSITE STRUCTURES USING EXPERIMENTAL TECHNIQUES**” completed by **ALTAY OZANKAN** under supervision of **ASSOC. PROF. DR. ABDULLAH SEÇGİN** and we certify that in our opinion it is fully adequate, in scope and in quality, as a thesis for the degree of Master of Science.



Assoc. Prof. Dr. Abdullah SEÇGİN

Supervisor



Prof. Dr. A. Saide Sangül

(Jury Member)



Yrd. Doç. Dr. Mehmet SARIKAVAT

(Jury Member)



Prof. Dr. Ayşe OKUR

Director

Graduate School of Natural and Applied Sciences

ACKNOWLEDGMENTS

This thesis with the title “*Vibro-Acoustic analysis of uncertain composite structures using experimental techniques*” is one of the outcomes of 112M836 numbered project supported by The Scientific and Technological Research Council of Turkey, TUBİTAK.

I would like to present my sincere appreciation to my thesis advisor Assoc. Prof. Dr. Abdullah SEÇGİN for all his patience and efforts in my entire master education. His guidance and countless critical suggestions helped me to finish this project.

I would also like to thank Prof. Dr. A. Saide SARIGÜL and my friends Murat KARA, Muzaffer KASABA, Yusuf İHTİYAROĞLU and Burak Emre YAPANMIŞ.

Finally, thanks to my mother Birsen GÖLLER and my aunt Selma GÖLLER for their support in my entire education.

Altay OZANKAN

VIBRO-ACOUSTIC ANALYSIS OF UNCERTAIN COMPOSITE STRUCTURES USING EXPERIMENTAL TECHNIQUES

ABSTRACT

Vibro-acoustic experiments provide a basis for all predictive analysis methods and also provide more realistic predictions especially for very complex systems. They are also utilized for the verification purposes for numerical, semi-analytical and energy based methods.

This thesis aims to give application procedures of various experimental techniques. The studies in the thesis are an important part of a national project aiming for developing an efficient mid and high frequency method. Here, comprehensive application procedures of experimental modal analysis, experimental power injection method (PIM), accelerance, receptance and mobility measurements for simple and more complex composite structures are presented.

Beside this, experimental uncertainty analyses are performed and discussed in detail in the thesis. The effects of structural variations causing vibro-acoustic uncertainty are obtained via experimental Monte Carlo simulations from simple to very complex structures such as single plate to a cabinet.

Keywords: Uncertainty, experimental Monte Carlo simulation, statistical energy analysis, finite element analysis, power injection method, laminated composite plates, acoustic cavity.

BELİRSİZ KOMPOZİT YAPILARIN DENEYSSEL YÖNTEMLERLE VİBRO- AKUSTİK ANALİZİ

ÖZ

Deneysel vibro-akustik analizler diğer tahminleme analiz yöntemlerine temel oluşturmaktadır. Ayrıca, karmaşık yapıların cevap tahminlerinde daha gerçekçi sonuçlar vermektedir. Bu analizler sayısal, yarı-analitik ve enerji tabanlı yöntemlerin doğrulama çalışmalarında da kullanılmaktadır.

Bu tez, çeşitli deneysel tekniklerin uygulama usullerini göstermek amacıyla yazılmıştır. Tezde yapılan çalışmalar orta ve yüksek frekans bölgesinde etkili bir yöntem geliştirmeyi amaçlayan ulusal bir araştırma projesinin önemli bir parçasını oluşturmaktadır. Bu tezde, basit sistemlerden oldukça karmaşık sistemlere doğru gelişen deney düzeneklerine uygulanan deneysel modal analiz, deneysel güç enjeksiyon yöntemi, akselerans, reseptans, mobilite ölçümlerinin uygulama esasları sunulmuştur.

Bunun yanı sıra, deneysel belirsizlik analizleri yapılmış ve tez içerisinde detaylıca tartışılmıştır. Yapısal değişkenliklerin neden olduğu vibro-akustik belirsizlik deneysel Monte Carlo simülasyonu yöntemiyle tek plakadan, bir kabin sistemine doğru gittikçe karmaşıklaşan deney yapılarına uygulanmıştır.

Anahtar kelimeler: Belirsizlik, deneysel Monte Carlo simülasyonu, istatistiksel enerji analizi, sonlu elemanlar analizi, güç enjeksiyon yöntemi, katmanlı kompozit plakalar, akustik hacim.

CONTENTS

	Page
THESIS EXAMINATION RESULT FORM	ii
ACKNOWLEDGEMENTS	iii
ABSTRACT	iv
ÖZ	v
LIST OF FIGURES	viii
LIST OF TABLES	xii
CHAPTER ONE - INTRODUCTION	1
CHAPTER TWO - METHODS.....	9
2.1 Modal Analysis	9
2.1.1 Experimental Modal Analysis.....	9
2.1.1.1 Single Degree of Freedom Approach.....	10
2.1.1.1.1. Peak Selection Method.....	12
2.1.1.1.2. Circle Fit Method	14
2.1.2 Bending Vibrations of a Thin Composite Plate	14
2.2 Statistical Energy Analysis (SEA)	15
2.2.1 Coupling Loss Factor (CLF) and Damping Loss Factor (DLF)	16
2.2.1.1 Average Modal Spacing (AMS)	20
2.2.1.2 Power Input	21
2.2.1.3 Infinite System Impedance.....	21
2.2.2 Modal Overlap Factor (MOF).....	22
2.2.3 Power Balance In SEA Analysis.....	23

2.3 Power Injection Method (PIM)	24
2.4 Monte Carlo Simulation.....	27
CHAPTER THREE - MODAL ANALYSIS	28
3.1 Modal Analysis of a Beam.....	28
3.2 Modal Analysis of a Composite Plate.....	29
3.2.1 The Composite Plate	30
3.2.2 Experimental Modal Analysis.....	31
3.3 Modal Analysis of a T-type Structure.....	33
3.3.1 Numerical Modal Analysis	34
3.3.2 Experimental Modal Analysis.....	35
CHAPTER FOUR - DETERMINATION OF SEA PARAMETERS OF STRUCTURES.....	40
4.1 Determination of the DLF of an Aluminum Beam	40
4.2 Determination of the DLF of a Single Composite Plate	41
4.3 Calculation of SEA Parameters of I-, L-,T- Type Structures.....	42
CHAPTER FIVE - UNCERTAINTY ANALYSES	47
5.1 Uncertainty Analysis of A Single Composite Plate	47
5.1.1 Effect of Uncertainty on Natural Frequencies	49
5.1.2 Effect of Uncertainty on Frequency Response Function	50

5.2 Uncertainty Analysis of T-type Structure	53
5.3 Uncertainty Analysis of Stiffened Plate	58
5.3.1 MOF values and High Frequency Thresholds	59
5.3.2 Vibration Velocity Response of Uncertain Stiffened Plate.....	60
5.4 Uncertainty Analysis of Structural-Acoustic System: Cabinet.....	65
5.4.1 Manufacturing of the Cabinet	67
5.4.2 Free Vibration Analysis of the Cabinet.....	70
5.4.3 Frequency Response Function of the Cabinet.....	72
5.4.4 Uncertainty Analysis of the Cabinet	72
CHAPTER SIX - CONCLUSION	76
REFERENCES.....	78
APPENDICES	83
Appendix A	83
Appendix B	84
Appendix C	85

LIST OF FIGURES

	Page
Figure 2.1 Quality factor	13
Figure 2.2 Modal spacing representation of a frequency response function	20
Figure 2.3 A SEA model of two connected subsystems	23
Figure 3.1 Aluminum hollow beam	28
Figure 3.2 Accelerance response of the aluminum hollow beam with predicted natural frequencies	29
Figure 3.3 Experimental modal analysis setup	30
Figure 3.4 Modal analysis results of the composite plate.....	31
Figure 3.5 Frequency response function of the five-DOF composite plate model ..	33
Figure 3.6 T-type structure with point connections	34
Figure 3.7 Numerical model of the T-type structure	35
Figure 3.8 Experimental modal analysis setup of the T-type structure	36
Figure 3.9 Transfer receptances of composite structure a) first half, b) second half	37
Figure 4.1 Aluminum hollow beam	40
Figure 4.2 Damping loss factor of the beam	41
Figure 4.3 Experimental setup for the determination of damping loss factor	42
Figure 4.4 Damping loss factor of the plate	42
Figure 4.5 Composite structures a) I-type, b) L-type, c) T-type	43
Figure 4.6 Experimental setup for power injection method	44
Figure 4.7 Loss factors of I-type composite structure (blue line: experimental, dashed: numerical, grey: single plate (from Figure 4.4), dotted: SEA) ..	44
Figure 4.8 Loss factors of L-type composite structure (blue line: experimental, dashed: numerical, grey: single plate (from Figure 4.4), dotted: SEA) ..	45
Figure 4.9 Loss factors of T-type composite structure (blue line: experimental, dashed: numerical, grey: single plate (from Figure 4.4), dotted: SEA) ..	46
Figure 5.1 Driving points of the plate	47
Figure 5.2 Thickness samples of the plate.....	49
Figure 5.3 Uncertainty effect on natural frequencies	50

Figure 5.4	Schematic representation of driving points and locations of added masses (o: driving points, Δ : randomly located measurement points)	51
Figure 5.5	Experimental setup of uncertainty analysis	51
Figure 5.6	Experimental driving points mobilities of the plate (grey: uncertain result of 60; dashed dot: mean experimental result of driving points; dashed line: infinite system mobility)	52
Figure 5.7	Experimental transfer mobilities of the plate (grey: uncertain result of 60; dashed dot: mean experimental result of transfer points)	52
Figure 5.8	Experimental and numerical uncertainty results of T-Type structure a) subsystem 1 b) subsystem 2 c) subsystem 3 (grey: experimental uncertainty results, blue line: mean experimental uncertainty results, red line: mean numerical uncertainty results)	54
Figure 5.9	Response comparison of subsystem 1 in T-type structure a) 10-1000 Hz, b) 1000-5000 Hz (blue line: experimental Monte Carlo mean, dashed: experimental SEA, red: FEM-Monte Carlo mean, dotted: analytical SEA)	55
Figure 5.10	Response comparison of subsystem 2 in T-type structure a) 10-1000 Hz, b) 1000-5000 Hz (blue line: experimental Monte Carlo mean, dashed: experimental SEA, red: FEM-Monte Carlo mean, dotted: analytical SEA)	56
Figure 5.11	Response comparison of subsystem 3 in T-type structure a) 10-1000 Hz, b) 1000-5000 Hz (blue line: experimental Monte Carlo mean, dashed: experimental SEA, red: FEM-Monte Carlo mean, dotted: analytical SEA)	57
Figure 5.12	Stiffened plate	59
Figure 5.13	MOF values of structures and high frequency thresholds	60
Figure 5.14	Stiffened plate and added mass distribution sample.....	61
Figure 5.15	Frequency response function of the plate a) 10-500 Hz, b) 500-5000 Hz	62
Figure 5.16	Frequency response function of the 1st beam a) 10-500 Hz, b) 500-5000 Hz	63

Figure 5.17 Frequency response function of the 2nd beam a) 10-500 Hz, b) 500-5000 Hz	64
Figure 5.18 Design of the cabinet a) chassis, b) chassis + plates	66
Figure 5.19 Dimensions of the cabinet design	66
Figure 5.20 Manufactured cabinet model a) cabinet, b) position of vibration motor and damping material	67
Figure 5.21 Structural SEA model of the cabinet SEA.....	69
Figure 5.22 FRF of the excitation implemented to the cabinet a) acceleration, b) force	72
Figure 5.23 Experimental uncertainty setup of the cabinet	73
Figure 5.24 Acceleration responses of the uncertain plate (28 th subsystem) (grey: uncertainty results, blue line: experimental uncertainty mean, black dashed: FEM results, red dotted: analytical SEA)	74
Figure 5.25 Sound pressure levels of the acoustical cavity (grey: uncertainty results, blue line: experimental uncertainty mean, black dashed: FEM results, red dotted: analytical SEA)	74

LIST OF TABLES

	Page
Table 2.1 AMS for some different subsystems	21
Table 2.2 Driving point impedance of structures	22
Table 3.1 Mechanical properties of the beam	28
Table 3.2 Mechanical and physical properties of plate	30
Table 3.3 Natural frequencies, damping ratios, modal constants of the composite plate	32
Table 3.4 Experimental and numerical natural frequencies obtained from Peak Selection Method	39
Table 5.1 Brief of analyses made in the chapter	48
Table 5.2 Mechanical properties of the plate and beam.....	59
Table 5.3 Experimental uncertainty distribution.....	61
Table 5.4 Total mass of beam and plate used to construct the cabinet model	67
Table 5.5 Natural frequencies of the parts of the structure	71

CHAPTER ONE INTRODUCTION

Composite structures and materials are extensively used in aerospace and automobile industry for a while, due to their mechanical advantages such as strength/weight ratio, corrosion resistance, high impact strength, electrical resistivity, etc. Therefore, investigation of vibro-acoustic behaviors of these materials has an important place in engineering studies.

As it is well known, vibro-acoustic analyses are implemented in frequency domain generally. Also one can divide frequency domain into its three major parts; low, mid and high frequency regions. Conventional analysis methods are usually initiated for low frequency region. In this region resonated behavior dominates the response. For the determination of low frequency modal responses modal analysis can be used. Modal analysis applications were used extensively not only in mechanical engineering but also in different areas of engineering disciplines such as, civil, aeronautical, electronic, etc.

For instance, Clemente et al. used experimental modal analysis in order to determine modal behavior of a cable-stayed bridge (Clemente, Marulo, Lecce, & Bifulco, 1998).

Zhang et al. investigated modal response of a silicone sensor via modal analysis in order to validate the operation (Zhang, Tangi, Shan, Brandon, & Kwan, 1998).

Liang et al. implemented modal analysis to a suspension bridge in an attempt to reveal modal behavior of this structure (Liang, Jun, & Jing, 2001).

Also, Xu & Guo used experimental and numerical modal analysis in order to determine modal behavior of hard disk drive (Xu, & Guo, 2003).

By using recent technological developments researchers still use modal analysis techniques for modal behavior determinations of different kind of structures;

Chierichetti et al. used experimental modal data in order to monitor dynamic responses (Chierichetti, Grappasonni, Coppotelli, & McColl, 2014).

Batou et al. used experimental modal data in order to identify stochastic dynamic responses of one-stage pump (Batou, Soize, & Audebert, 2015).

Zhong et al. used optical coherence vibration tomography in order to determine low frequency vibrational behavior of structures which vibrates with nano scaled vibration displacements (Zhong, Zhong, & Zhang, 2016).

Oliveira et al. implemented experimental modal analysis by using piezoelectric transducers in order to determine modal characterization of composite plate structures (Oliveira, Maia, Marto, Silva, Afonso, & Suleman, 2016)

Hooper and Marco investigated modal behavior of Li-ion cells which are widely used in hybrid vehicles (Hooper, & Marco, 2016).

In high frequency region, frequency responses are getting smoother due to modal overlapping. Also the transition from the low to high frequencies is not linearly expressed, it exhibits a complex transition zone which is called as mid frequency region. Actually, there are no clear separations between these three regions. Only the threshold of high frequency region for simple structures can be approximately calculated via modal overlap factor (MOF) (Rabbiolo et al., 2004).

Increase in the usage of light-weighted composite materials to reduce fuel consumption or range enhancement elicits a shift in vibro-acoustic response through mid and high frequency regions. Numerical analysis methods such as FEM are generally used in industrial applications, which is a valid method for the determination of low frequency responses. In order to maintain valid predictions by these deterministic techniques in higher frequencies, excessive number of elements are required. This leads to high solution time and large memory usage. Therefore, special analysis methods should be considered for these higher frequencies.

In high frequency region, statistical and energy based methods are generally used. Statistical energy analysis (SEA) (Fahy, 1994; Lyon & DeJong, 1998, Keane & Price, 1997) is the most commonly used method in engineering areas. This analysis technique requires vibro-acoustic parameters of structures. For the determination of SEA vibro-acoustic parameters various methods were developed;

A steady state power input method called Power Injection Method (PIM) (Bies & Hamid, 1980; Langhe & Sas, 1996; Lalor, 1997; Manik, 1988) were widely implemented approach in order to determinate the loss factors of subsystems.

Also, several other methods were emerged in order to achieve the same result;

A FEM approach has been developed by Steel et al. for the investigation of structure-borne sound transmission (Steel & Craik, 1994).

Fahy et al. have developed a different method called input power modulation technique in order to determine these coefficients (Fahy & Ruivo, 1997).

A wave approach has been developed by McDaniel et al. for the estimation of frequency dependent loss factors in one dimensional structures (McDaniel, Dupont & Salvino, 2005).

Since Fahy argued about the loss factors were not the best indicators of internal energy dissipation and transfer between subsystems for the determination of energy levels (Fahy, 1998); suggested an alternative parameter, which was proportional to a derived parameter from modal densities and loss factors.

Ming experimentally investigated the parameter derived and the method developed by (Fahy, 1998) with such advantages; easier implementation and less measurement error (Ming, 2005). However, this method leads an approximate result due to its convenience.

Berthaut et al. have proposed a method called inhomogeneous wave correlation (IWC) for the identification of dispersion curves of two dimensional structures (Berthaut, Ichchou & Jezequel, 2005).

Maxit et al. have developed a dual formulation method for determination of loss factors by using FEM modal information (Maxit, & Guyader, 2009).

Also, for the estimation of loss factors of orthotropic two dimensional structures Cherif et al. proposed a method based on inhomogeneous wave correlation (Cherif, Chazot, & Atalla, 2015).

Seçgin et al. have recently determined loss factors in-situ via PIM of point connected composite structures (Seçgin, Güler, & Kara, 2015).

In mid frequency region, SEA and FEM could not individually provide efficient predictions. Therefore, researchers have focused on developing hybrid methods based on numerical and statistical methods;

Langley et al., (1998) have presented a technique, which contains SEA, fuzzy structure theory and Belyaev smooth function approach.

Vlahopoulos et al., (2001) have developed a hybrid Finite Element Analysis (FEA) technique for the demonstration of the importance of the resonance effects in mid frequency range.

Shorter et al., (2005) have presented a hybrid method that estimate vibrational behavior of complex systems and also applicable for non-reverberant subsystems.

Vanmaele et al., (2007) have developed a wave based method for mid frequency vibrations of plates.

Seçgin has developed a modal based approach for numerical determination of statistical energy analysis parameters of directly coupled composite structures (Seçgin, 2013).

Seçgin et al. have proposed a hybrid technique called modal impedance technique used for high frequency analysis of uncertain stiffened composite plate (Seçgin, Kara, & Ozankan, 2015).

Products that were manufactured in same production line may indicate different vibro-acoustical behavior due to uncertainty. This phenomenon may be emerged from small variations in geometry, material property, excitation characteristic, initial and boundary conditions of structures. Uncertainty incapacitates the traditional estimation techniques of response not only in low frequency region but mid and high frequency region too.

For lower frequencies, effect of uncertainty can be simulated via Monte-Carlo Simulation (Evans & Swartz, 2000; Fahy, 1994; Hobenbichler & Rackwitz, 1998; Lewis & Böhm, 1984).

However, energy based approaches such as SEA are capable of considering uncertainty effects in high frequency region. By these reasons energy based statistical approaches frequently used.

SEA and its subsidiary methods will be explained in the following chapter. Also, experimental methods for the determination of vibro-acoustic behavior of composite structures are performed in the applications.

Experimental methods take an important place for the prediction of vibro-acoustical behavior. Experimental measurements provide a basis for all predictive analysis methods. It is utilized also for the verifications of various numerical and analytical methods. As mentioned above numerical deterministic techniques and

statistical energy based techniques are only valid in different frequency regions. This consequence leads a lack of information in other ranges.

In this study, as a part of a national project aiming for developing an efficient mid and high frequency method, various experimental works were performed for verification purpose and also for providing the information to the other methods. In this regard, in this thesis, one can find comprehensive application procedures of experimental modal analysis, experimental power injection method (PIM), accelerance, receptance and mobility measurements for simple and more complex composite structures. Also, the study includes experimental Monte Carlo simulation to simulate mass uncertainty for simple to complex systems. In this study experimental vibro-acoustic analyses were made for simple and more complex composite structures in order to maintain a significant reference study for literature.

Especially, structural-acoustics analyses made for cabinet structure which is produced by composite subsystems were submitted for the first time in literature.

The thesis is organized as from six main chapters;

First chapter begins with an introduction section.

In Chapter 2, one can find the theoretical bases of various analytical, numerical and experimental methods.

Chapter 3 presents numerical and experimental modal analysis of various structures from simple to complex ones together with verification studies.

Chapter 4 concerns with experimental determination of statistical energy analysis parameters for several structures based on power injection method (PIM).

Chapter 5 is dedicated to the uncertainty analyses for several structures including a stiffened plate and a cabinet with acoustic volume by using numerical and experimental Monte Carlo analyses.

Finally, Chapter 6 ends up with a conclusion of the thesis.

This study is sponsored by the Scientific and Technological Research Council of Turkey (TÜBİTAK) with the project number 112M836. All the analytical and numerical data which compared with experimental results were taken from the report of this project. Also these data's in figures were indicated with the label "Tübitak Project Report, 112M836, 2015" in their annotations.

Symbol list:

k : stiffness constant	
c : damping constant	ρ_0 : mean mass density
m : mass	ν : Poisson ratio
f : frequency	D : rigidity matrix
t : time	a, b, h : dimensions of a rectangular plate
ω : angular frequency	Ω : dimensionless natural frequency parameter
τ : period	P : power input
ϕ : phase angle	E : vibration energy
h : hysteretic damping coefficient	$\overline{\delta f_i}$: average modal spacing
α : receptance	β_{corr} : modal coupling factor
η : structural damping loss factor	τ : power transmission
ξ : damping ratio	$\beta_{i,net}$: modal factor
ω_0 : natural frequency	$Z_{k\infty}$: infinite system impedance
j : $\sqrt{-1}$	
A : modal constant	

L_c : length of the connection	speed of waves
A_c : Area of the connection	Y_0 : driving point mobility
θ, ϕ : incidence angles	$F(\omega), M(\omega)$: frequency
$I_{i,j}^{line(area)}$: integral factor	dependent force and moment
E_y : Young modulus	c_L : longitudinal wave speed (in Table 2.2)
G : shear modulus	c_b : bending wave speed
μ : Poisson ratio (in Table 2.1)	k_L : longitudinal stiffness
ρ : density	k_b : bending stiffness
κ : radius of gyration	r : radius of excitation
L : length	$\langle \overline{E_i} \rangle$: time, spatial, frequency
A : area	average of energy
V : volume	$\langle \overline{P_i} \rangle$: time, spatial, frequency
J : torsional rigidity	average of pressure
I_x, I_y : area moments of inertia	$\langle \overline{v_i} \rangle$: time, spatial, frequency
about x and y axis	average of velocity
I_p : summation of moments of inertia	E_{tot} : total energy
c_{Lx}, c_{Ly} : longitudinal wave speed	
towards x and y axis	
c_L : geometrical mean of the	

CHAPTER TWO THEORY

In this section, methods used in this thesis, are explained. In this regard, experimental modal analysis and statistical energy analysis (SEA) which is used for high frequency vibro-acoustic analysis are given. Here, a power injection method to determine the SEA parameters is also briefly presented. Chapter finalizes by experimental uncertainty simulation for vibro-acoustic structures.

2.1 Modal Analysis

Modal analysis is simply the process of determining the essential vibration characteristics, i.e, natural frequency, damping ratio, modal constant and mode shape, to compose the mathematical model indicating dynamical behaviour of a vibrating structure. This test can be performed analytically for simple structures such as beams and plates. However, there no analytical solution is available for complicated structures. In these cases, numerical or experimental modal analyses should be performed.

2.1.1 *Experimental Modal Analysis*

Experimental modal analysis systems are composed of contact (accelerometers, load cells etc.) or non-contact transducers (laser vibrometers, stereophotogrammetric cameras), data acquisition systems, analog to digital converters (ADC) and computers.

Mechanical systems can be modeled as single degree of freedom (SDOF) or multi degree of freedom (MDOF) systems. MDOF system can be modeled as superposition of several SDOF systems via linear vibration theory. In experimental modal analysis complex systems can be analyzed by both SDOF and MDOF approach methods. In this study SDOF Peak Selection Method was used in the analyses. Peak selection method and Circle fit method are generally used for SDOF approach whereas curve fitting method is the most common for MDOF approach.

In SDOF approach, peak selection is mostly preferred method since it leads to immediate evaluation of response with an easy application. This method is also known as half power method. Modal parameters can be obtained by an analysis of sufficiently wide band of the receptance peak at the resonance frequency. In circle fitting method, modal parameters are determined from composed circular relation by plotting real and imaginary part of the receptance (Nyquist diagram). In the thesis, peak selection method is used in modal analyses works, (He & Fu, 2001). In curve fitting, frequency response function (FRF) curve of the receptance approximately defined as various mathematical functions. In this process, fracture polynomials or complex exponential curve forms are generally used.

There are three widely used FRF parameters exists. Receptance is the ratio of the displacement over the force. Mobility is the ratio of the velocity over the force. Accelerance is ratio of the acceleration over the force. Here, it is worthy to point out that, in measurements performed in studies, all these parameters were selected to be measured for following reasons: Accelerance was measured in the modal analysis of a beam, since acceleration data can be easily measured and there was no comparison required. Receptances were measured for comparison purpose of some structures, since those structures already have analytical displacement responses. Mobilities were measured for the comparison studies with SEA, since SEA parameters are generally obtained from impedances which are the inverse of mobilities.

For modal analyses, SDOF approach is used in easy and quick evaluation of the modal information for low damped systems. However, MDOF approach can be used at all damped systems and more complex structures for determination of more reliable modal information.

2.1.1.1 Single Degree of Freedom Approach

SDOF systems can be modeled as a spring with a stiffness constant \mathbf{k} , a damper with a damping constant \mathbf{c} and an element with a mass \mathbf{m} . For harmonic force excitation at frequency ω , $(f(t) = F(\omega)e^{j\omega t})$ the response of the system can be

assumed as $(x(t) = X(\omega)e^{j\omega t})$, where $\omega\tau = \phi$ is phase between force and response.

Receptance response of the system can be represented as; (He, & Fu, 2001)

For viscous damping:

$$\frac{X(\omega)}{F(\omega)} = \frac{1}{k - \omega^2 m + j\omega c} . \quad (2.1)$$

For structural damping:

$$\frac{X(\omega)}{F(\omega)} = \frac{1}{k - \omega^2 m + jh} . \quad (2.2)$$

Here, $h = \omega c$ is hysteretic damping coefficient. Receptance (α) is the ratio of displacement over force that applied to the system. Equation (2.1) and (2.2) can be rewritten with modal parameters as; (He, & Fu, 2001)

For viscous damping:

$$\alpha(\omega) = \frac{1/m}{\omega_0^2 - \omega^2 + 2j\omega\omega_0\xi} . \quad (2.3)$$

For structural damping;

$$\alpha(\omega) = \frac{1/m}{\omega_0^2 - \omega^2 + j\omega_0^2\eta} . \quad (2.4)$$

In these formulas, ω_0 is the natural frequency, ω is the excitation frequency, ξ is damping ratio and η is structural damping loss factor of the SDOF system, given as h/k .

2.1.1.1.1. Peak Selection Method

Frequency response function of a system having several modes can be determined by using Equation (2.3) as follows;

$$\alpha(\omega) = \sum_{n=1}^N \frac{A_n}{\omega_n^2 - \omega^2 + 2j\omega\omega_n\xi_n} \quad (2.5)$$

And for small damped systems;

$$\alpha(\omega) = \sum_{n=1}^N \frac{A_n}{\omega_n^2 - \omega^2} \quad (2.6)$$

Modal parameters can be calculated as;

Frequency response function value at the peak is expressed as $\alpha_{\max} = \frac{A_n}{2\xi_n\omega_n^2}$. Here

the modal constant A_n , indicating that the amount of response contribution of nth mode, can be estimated as

$$A_n = 2 \cdot \alpha_{\max} \cdot \xi_n \cdot \omega_n^2, \quad (= \alpha_{\max} \cdot \eta_n \cdot \omega_n^2) \quad (2.7)$$

Viscous damping ratio can be derived from modal bandwidth (quality factor). Quality factor is a dimensionless parameter of the bandwidth frequency values which is 3 dB less than the peak value (Figure 2.1).

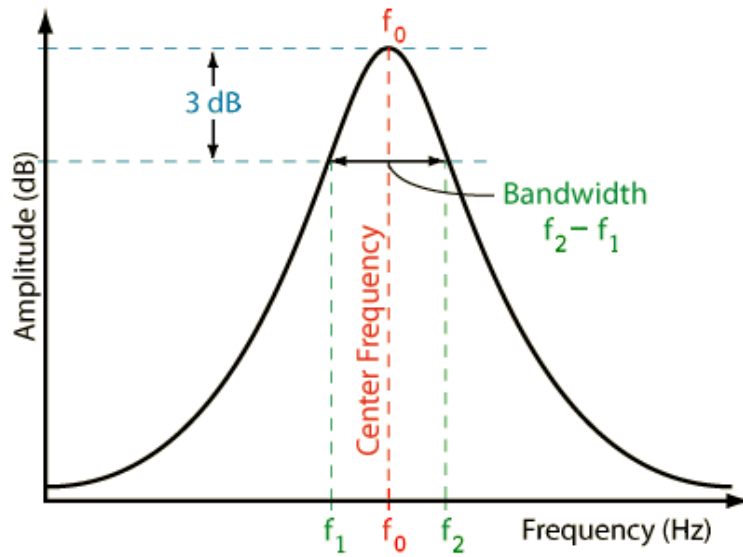


Figure 2.1 Quality factor

Viscous damping ratio;

$$\xi_n = \frac{f_2 - f_1}{2f_0} . \quad (2.8)$$

Structural damping ratio;

$$\eta_n = \frac{f_2 - f_1}{f_0} . \quad (2.9)$$

Peak value:

$$\alpha_{\max} = |\alpha_n(\omega_n)_{\max}| . \quad (2.10)$$

In Equations (2.8) - (2.10) f_1 and f_2 are lower and higher frequency of modal bandwidth respectively where f_0 center frequency of the band.

2.1.1.1.2. Circle Fit Method

Circle Fit method is one of the most used SDOF modal analysis method. It is based on the circularity of the Nyquist diagram of an SDOF system. With the effect of structural damping, receptance FRF traces a circle on Nyquist diagram having form of (He & Fu, 2001) :

$$(\text{Re}(\alpha))^2 + \left(\text{Im}(\alpha) + \frac{1}{2h} \right)^2 = \left(\frac{1}{2h} \right)^2 \quad . \quad (2.11)$$

2.1.2 Bending Vibrations of a Thin Composite Plate

Deflection in Cartesian coordinates for time independent equation of motion of a thin symmetrically layered composite plate can be written as (Whitney, 1987).

$$\begin{aligned} D_{11} \frac{\partial^4 w(x, y)}{\partial x^4} + 4D_{16} \frac{\partial^4 w(x, y)}{\partial x^3 \partial y} + 2(D_{12} + 2D_{66}) \frac{\partial^4 w(x, y)}{\partial x^2 \partial y^2} \\ + D_{26} \frac{\partial^4 w(x, y)}{\partial x \partial y^3} + D_{22} \frac{\partial^4 w(x, y)}{\partial y^4} - \rho_0 h \omega_n^2 w(x, y) = 0. \end{aligned} \quad (2.12)$$

Here, a and b are plate dimensions, h is total thickness, ρ_0 is mean mass density, ν is Poisson ratio, D_{11} , D_{12} , D_{22} and D_{66} are bending rigidities in the principle direction of material, D_{16} and D_{26} are the rigidities of the bending-torsion pair.

Boundary conditions for simply-supported system (SSSS) can be given as (Whitney, 1987).

$$\text{At } x=0, a; w = 0 : \quad -D_{11} \frac{\partial^2 w}{\partial x^2} - 2D_{16} \frac{\partial^2 w}{\partial x \partial y} - D_{12} \frac{\partial^2 w}{\partial y^2} = 0, \quad (2.13a)$$

$$\text{At } y=0, b; w = 0 : \quad -D_{12} \frac{\partial^2 w}{\partial x^2} - 2D_{26} \frac{\partial^2 w}{\partial x \partial y} - D_{22} \frac{\partial^2 w}{\partial y^2} = 0, \quad (2.13b)$$

Equation (2.12) can be rewritten, through dimensionless parameters represented as: $X = x/a$, $y = Y/b$, $W = w/a$, $\lambda = a/b$, $D_\gamma = (D_{11}/D_{22})$, $D_\phi = (D_{12} + 2D_{66})/D_{22}$, $D_\alpha = (D_{16}/D_{22})$, $D_\beta = (D_{26}/D_{22})$.

$$D_\gamma \frac{\partial^4 W(X,Y)}{\partial X^4} + 2\lambda^2 D_\phi \frac{\partial^4 W(X,Y)}{\partial X^2 \partial Y^2} + \lambda^4 \frac{\partial^4 W(X,Y)}{\partial Y^4} + 4(\lambda D_\alpha \frac{\partial^4 W(X,Y)}{\partial X^3 \partial Y} + \lambda^3 D_\beta \frac{\partial^4 W(X,Y)}{\partial X \partial Y^3}) - \Omega^2 W(X,Y) = 0, \quad (2.14)$$

In this formula, $\Omega = \omega a^2 \sqrt{\rho_0 h / D_{22}}$ is dimensionless natural frequency parameter. Equation (2.14) can be simplified for special orthotropic and isotropic plates depending on two features;

1- For special orthotropic plates: Symmetrically 0° and 90° orientation angle layered plates; rigidities become $D_\gamma \neq D_\phi$ and $D_\alpha = D_\beta = 0$ ($D_{16} = D_{26} = 0$).

2- For isotropic plates; rigidities become $D_\gamma = D_\phi = 1$ and $D_\alpha = D_\beta = 0$ ($D_{11} = D_{22} = D = Eh^3 / 12(1 - \nu^2)$ and $D_{16} = D_{26} = 0$).

Analytical dimensionless natural frequency parameter for plates, which have simply supported boundary condition, can be defined as;

$$\Omega_{p,q} = \omega_{p,q} a^2 \sqrt{\frac{\rho_0 h}{D_{22}}} = \pi^2 \sqrt{p^4 D_\gamma + 2p^2 q^2 \lambda^2 D_\phi + q^4 \lambda^4} \quad \text{where } p, q = 1, 2, \dots \quad (2.15)$$

2.2 Statistical Energy Analysis (SEA)

Statistical energy analysis (SEA) is a high frequency dynamic analysis method developed by R.H. Lyon (SEA) (Fahy, 1994; Lyon & DeJong, 1998) in early 1960s. In this method complex structures are divided into subsystems and then power balance is provided between these subsystems. Mean energy values are calculated for these subsystems and dynamic responses such as velocity, acceleration and pressure

can be evaluated from these mean energy values. Analytical SEA has many limitations and assumptions such as high modal density, non-localized damping, and having equal energy magnitude for each vibration resonance.

Since SEA calculates the statistical parameters (mean, standard deviation) of response, it can automatically take uncertainties into account. However, in this method each subsystem should have sufficient number of vibro-acoustic modes to define accurately the system. The success of SEA also depends on the accurate prediction of its parameters, i.e, coupling loss factor (CLF), damping loss factor (DLF), average modal spacing (AMS) and power input.

2.2.1 Coupling Loss Factor (CLF) and Damping Loss Factor (DLF)

CLF and DLF present the amount of power transmission between subsystems and power absorption of subsystems, respectively. CLF can be evaluated with analytical methods for simple structures by using finite/semi-infinite system impedances (Lyon & DeJong, 1998) or dual modal formulation (Maxit & Guyader, 2009a, 2009b) but it can be evaluated by numerical/experimental power injection method for complex structures whereas DLF is determined via some experimental methods such as logarithmic decrement, quality factor (Lyon & DeJong, 1998; Rao, 1995), decay rate method (Bloss & Rao 2005; Lyon & DeJong, 1998) and power injection method (PIM) (Bies & Hamid, 1980; Langhe & Sas, 1996).

SEA equations are written by setting power balance between subsystems. A subsystem dissipates energy as:

$$P_i = \omega \eta_i E_i . \quad (2.16)$$

where ω is angular frequency of vibration, η_i is damping loss factor (DLF), E_i is vibration energy of i^{th} subsystem. Power transmission from i^{th} subsystem to j^{th} subsystem is expressed as:

$$P_{ij} = \omega \eta_{ij} E_i . \quad (2.17)$$

where η_{ij} , coupling loss factor (CLF) between i^{th} subsystem to j^{th} subsystem. Analytical CLF is determined using power transmission coefficient which can be derived either wave approach or modal approach. In wave approach incident, reflection and transmission at a joint is considered for the computational CLF. However, in modal approach, average energies obtained from modal information are used in computations. In the thesis, wave approach formulas are used. CLF can be expressed as (Lyon & DeJong, 1998):

$$\bar{\eta}_{ij} = \frac{\delta \bar{f}_i}{\pi f} \beta_{corr} \frac{\tau_{ij}}{2 - \tau_{ij}} . \quad (2.18)$$

In this formula, $\delta \bar{f}_i$, average modal spacing (AMS), β_{corr} , modal coupling factor, τ_{ij} , power transmission coefficient between i^{th} and j^{th} subsystem. Beside that,

Average Modal Spacing (AMS) can be used in the calculation of the CLF for two connected structures (Lyon & DeJong, 1998):

$$\bar{\eta}_{ij} = \frac{\delta \bar{f}_i}{\pi f} \beta_{corr} \frac{\tau_{ij}}{2 - \tau_{ij}} . \quad (2.19)$$

Here, $\delta \bar{f}_i$ is average modal spacing of subsystem i and modal coupling factor can be given as (Lyon & DeJong, 1998):

$$\beta_{corr} = \frac{1}{\left(1 + \left(\frac{1}{2\pi(\beta_{1,net} + \beta_{2,net})} \right)^8 \right)^{\frac{1}{4}}} . \quad (2.20)$$

Modal factor $\beta_{1,net}$ can be calculated as $f \eta_{i,net} / \delta \bar{f}_i$ in terms of net loss factor of subsystem i . Iteration is used for more accurate determination of coupling loss factor

CLF. In the iteration procedure, firstly, DLF is selected as initial CLFs and then by iteration, net loss factors are determined for each substructures.

Transmission coefficient can be represented in terms of infinite system impedances (Lyon & DeJong, 1998):

$$\tau_{ij}(0) = \frac{4 \cdot R_{i\infty} \cdot R_{j\infty}}{\left| \sum_{k=1}^m Z_{k\infty} \right|^2} . \quad (2.21)$$

Here, $Z_{k\infty}$ is infinite subsystem impedances at junction points, $R_{i\infty}$ and $R_{j\infty}$ are real parts of those impedances.

Transmission coefficient varies in accordance with the junction type; point, line and area connections.

For point connection junctions, Equation (2.20) should be used. However, transmission coefficient (and CLF) are affected by the angle of incidence wave for line and area connections (Lyon & DeJong, 1998):

$$\eta_{ij}^{line}(\theta) = \frac{\delta \bar{f}_i k_i L_c \cos(\theta)}{\pi f} \frac{\tau_{ij,\infty}(\theta)}{2 - \tau_{ij,\infty}(\theta)} \quad (2.22)$$

$$\eta_{ij}^{area}(\phi) = \frac{\delta \bar{f}_i k_i A_c \cos(\phi)}{\pi f} \frac{\tau_{ij,\infty}(\phi)}{2 - \tau_{ij,\infty}(\phi)} . \quad (2.23)$$

Here, L_c indicates length of connection between subsystems, A_c , area of connection between subsystems. Mean of the CLF along all incidence angle must be known to obtain frequency dependent CLF.

This situation depends on the assumption of the energy is homogenized along the incidence angles (Lyon & DeJong, 1998):

$$\langle \eta_{ij} \rangle_{\theta} = \frac{2}{\pi} \int_0^{\pi/2} \eta_{ij}(\theta) d\theta , \quad (2.24)$$

and

$$\langle \eta_{ij} \rangle_{\phi} = \int_0^{\pi/2} \eta_{ij}(\phi) \sin(\phi) d\phi , \quad (2.25)$$

Equation (2.24) and (2.25) can be rewritten independently from the incidence angle (Lyon & DeJong, 1998):

$$\bar{\eta}_{ij} = \frac{\delta \bar{f}_i}{\pi f} \beta_{corr} \cdot I_{ij}^{line(area)}(k_i, k_j) \cdot \frac{\tau_{ij}(0)}{2 - \tau_{ij}(0)} . \quad (2.26)$$

In this formula, $I_{ij}^{line(area)}$ represents the integral factor of the connection and $\tau_{ij}(0)$ is the transmission loss when the incidence angle of the wave to the junction. Besides, impedance of the Eq. (2.4) must be written for unit length and area in the expression of CLF for line and area connections.

Integral factor of line and area connection of plate and acoustic cavity were represented respectively (Lyon & DeJong, 1998):

$$I_{p \rightarrow c}^{line} = \frac{2}{\pi} \frac{k_0 k_p^2 L_s}{\left(\frac{\pi}{2}\right) k_0^2 + k_p^2} , \quad (2.27)$$

$$I_{p \rightarrow c}^{area} = \frac{\frac{A_p k_0^6}{8\pi k_p^4}}{\sqrt{\left(1 - \frac{k_0^2}{k_p^2}\right)^2 \left(1 + \frac{k_0^4}{\pi k_p^4}\right)^2 + \frac{2}{\pi k_p \sqrt{A_p}}}} \quad (2.28)$$

2.2.1.1 Average Modal Spacing (AMS)

Average modal spacing (AMS, $\delta\bar{f}$) shows average distance of two modes in terms of Hertz of a subsystem as shown in Figure 2.2. In Table 2.1, AMSs of some subsystems are compiled for several waveguides.

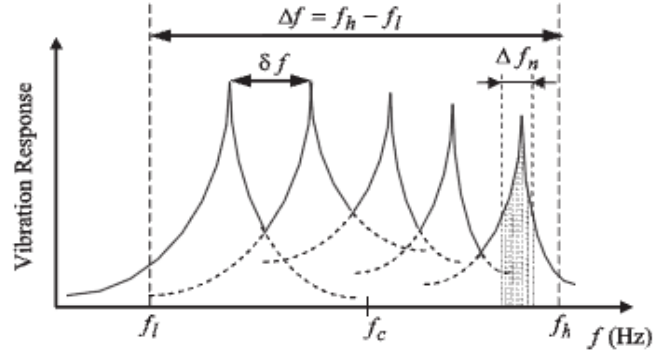


Figure 2.2 Modal spacing representation of a frequency response function (Seçgin & Sarigül, 2009)

In table 2.1, E_y represents Young Modulus, G is Shear Modulus, μ is Poisson Ratio, ρ is density, κ is radius of gyration, L is the length of the bar, A is the area of the plate, V is the volume of the acoustic cavity and $J = 4I_x I_y / (I_x + I_y)$ is torsional rigidity, $I_p = I_x + I_y$, I_x and I_y are the summation of area moments of inertia. Speed of wave can be obtained by the geometrical mean of the speed of waves towards at least 2 different directions ($c_L = \sqrt{c_{Lx} \cdot c_{Ly}}$) for orthotropic structures

Table 2.1 AMS for some different subsystems, compiled from (Lyon & DeJong, 1998)

Structure	Wave Guide	Average Modal Spacing	Speed of Wave
Bar	Longitudinal	$\frac{c_L}{2L}$	$c_L = \sqrt{E_y/\rho}$
	Torsional	$\frac{c_T}{2L}$	$c_T = \sqrt{GJ/\rho I_p}$
	Bending	$\frac{c_B}{L}$	$c_B = \sqrt{2\pi f \kappa c_L}$
Plate	Longitudinal	$\frac{c_L'^2}{2\pi f A}$	$c_L' = \sqrt{E_y/\rho(1-\mu^2)}$
	Shear	$\frac{c_S^2}{2\pi f A}$	$c_S = \sqrt{G/\rho}$ $G = E_y/(2(1+\mu))$
	Bending	$\frac{2\kappa c_L'}{A}$	$c_L' = \sqrt{E_y/\rho(1-\mu^2)}$
Acoustical Cavity	---	$\frac{c_{air}^3}{4\pi V f^2}$	$c_{air} = 20.05\sqrt{{}^oC + 273.15}$

2.2.1.2 Power Input

Spectral power input ($P_{i,in}$) of the subsystem can be determined as superposition of force and moment excitations:

$$P_{in}^{tot} = P_{in}^F + P_{in}^M = (F(\omega))^2 \operatorname{Re}\{Y_0^F\} + (M(\omega))^2 \operatorname{Re}\{Y_0^M\}. \quad (2.29)$$

Here, Y_0 , driving point mobility is the inverse of the system impedance. $F(\omega)$ and $M(\omega)$ are frequency dependent force and moments respectively.

2.2.1.3 Infinite System Impedance

Impedance can be defined as the ratio force over velocity. In Table 2.2, driving point impedances are given for basic waveguides. In Table 2.2, r represents radius of excitation and h denotes thickness of plate. However, for torsional and flexural

waveguides moment impedances are also exist. This impedance expression can be used in high frequency region, by the reason of vibrational wave reflections at the boundaries of the system are neglected. Since the energy of the higher frequency waves are relatively low, these waves absorbed by internal damping of the system and could not reflect.

In order to calculate transmission coefficients, impedances have to be adjusted according to boundary conditions. For example, point impedances for plate must be reduced by factor 2 for each free boundary and for beams by factor 4 under force excitation. Beside that acoustic impedance is reduced by factor 2 for each rigid boundary. For each pinned boundary, moment impedances are reduced by factor 2 (Lyon & DeJong, 1998).

Table 2.2 Driving point impedance of structures (Lyon & DeJong, 1998)

Subsystem, Waveguide	Force Impedance	Moment Impedance
Thin beam, flexural	$2\rho Ac_B(1+1j)$	$\frac{2\rho Ac_B}{k_B^2}(1-j)$
Thin plate, flexural	$8\rho h\kappa c'_L$	$\frac{16\rho h\kappa c_L/k_B^2}{1+j(4/\pi)\ln\left(1/k_B r\right)}$
Bar, longitudinal	$2\rho Ac_L$	---
Plate, inplane	$8\pi\rho hfr^2\left(1-\frac{j}{kr}\right)$	---
Bar, torsional	---	$2\rho I_p c_L$
Acoustic space	$\frac{\pi\rho f^2}{c}\left(1+\frac{j}{kr}\right)$	---

2.2.2 Modal Overlap Factor (MOF)

Structures should have high modal density for SEA applicability. In other words, demonstration of the vibration of the structure at high frequency region relies on a

statistical parameter called Modal Overlap Factor (MOF) (Lyon & DeJong, 1998). MOF is basically defined as the modal density in a modal bandwidth (Δf_n) (Figure 2.2). Beside that, MOF can be expressed as:

$$MOF = \frac{\pi f \eta}{2 \delta f} \quad (2.30)$$

Determination of MOF can be quite exhausting for complex structures. However, it can be approximately determined by experimental and statistical methods. Rabbiolo et. al. (2004) defined MOF as a high frequency indicator and relates MOF and high frequency threshold as 1 for bars, 2.5 for plates and 3 for acoustical cavities.

2.2.3 Power Balance In SEA Analysis

In Figure 2.3 an example SEA model of 2 connected subsystems is shown.

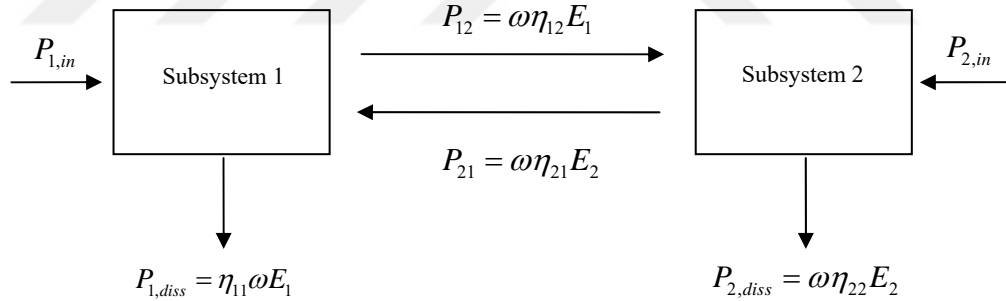


Figure 2.3 A SEA model of two connected subsystems

Power balance equations for each subsystem can be given as;

$$\frac{1}{\omega} \begin{Bmatrix} P_{1,in} \\ P_{2,in} \end{Bmatrix} = \begin{bmatrix} \eta_{11} + \eta_{12}^{line} + \eta_{12}^{area} & -(\eta_{21}^{line} + \eta_{21}^{area}) \\ -(\eta_{12}^{line} + \eta_{12}^{area}) & \eta_{22} + \eta_{21}^{line} + \eta_{21}^{area} \end{bmatrix} \begin{Bmatrix} E_1 \\ E_2 \end{Bmatrix} \quad (2.31)$$

Here, the matrix including CLFs and DLFs of subsystem is called as SEA matrix. One can evaluate the energies of each subsystem by multiplying inverse of SEA

matrix by power vector. Then dynamic parameters such as velocity for vibrating structures and pressure for acoustical subsystems can be determined as:

$$\langle \bar{v}_i \rangle = \sqrt{\langle \bar{E}_i \rangle / m_i}, \quad (2.32)$$

$$\langle \bar{p}_i \rangle = \sqrt{\langle \bar{E}_i \rangle \rho_i c_i^2 / V_i}. \quad (2.33)$$

Here, m_i is the mass of subsystem i , V_i is the volume of acoustic space, ρ_i is the density of air and c_i is the speed of sound.

2.3 Power Injection Method (PIM)

Power Injection Method (Bies & Hamid, 1980; Langhe & Sas, 1996) is generally applied to coupled structures to determine the DLF of subsystems and CLF between connected subsystems by measuring input power and energy amount of system. In this method;

1) Power input is applied to first subsystem and energy values are measured from all subsystems. In this case SEA equation (Bies & Hamid, 1980; Langhe & Sas, 1996) becomes,

$$\begin{Bmatrix} P_1 \\ 0 \\ \vdots \\ 0 \end{Bmatrix} = \omega \begin{bmatrix} \eta_{11}^0 & \eta_{12}^0 & \cdots & \eta_{1n}^0 \\ \eta_{21}^0 & \eta_{22}^0 & \cdots & \vdots \\ \vdots & \vdots & \ddots & \vdots \\ \eta_{k1}^0 & \cdots & \cdots & \eta_{kn}^0 \end{bmatrix} \begin{Bmatrix} E_{11} \\ E_{21} \\ \vdots \\ E_{k1} \end{Bmatrix}, \quad (2.34)$$

where E_{ij} is energy of i^{th} subsystem when j^{th} subsystem excited, P_j is power input of j^{th} subsystem, Equation (2.34) can also be rewritten in the form of:

$$\begin{Bmatrix} 1 \\ 0 \\ \vdots \\ 0 \end{Bmatrix} = \begin{bmatrix} \eta_{11}^0 & \eta_{12}^0 & \cdots & \eta_{1n}^0 \\ \eta_{21}^0 & \eta_{22}^0 & \cdots & \vdots \\ \vdots & \vdots & \ddots & \vdots \\ \eta_{k1}^0 & \cdots & \cdots & \eta_{kn}^0 \end{bmatrix} \begin{Bmatrix} E_{11}^n \\ E_{21}^n \\ \vdots \\ E_{k1}^n \end{Bmatrix}, \quad (2.35)$$

where E_{ij}^n is normalized energy of vibration and can stated as:

$$E_{ij}^n = \frac{\omega E_{ij}}{P_j}. \quad (2.36)$$

2) Afterwards second subsystem is excited and equation below can be obtained by measuring input power, energies of subsystems:

$$\begin{Bmatrix} 0 \\ 1 \\ \vdots \\ 0 \end{Bmatrix} = [\eta^0] \begin{Bmatrix} E_{12}^n \\ E_{22}^n \\ \vdots \\ E_{k2}^n \end{Bmatrix}. \quad (2.37)$$

Respectively this procedure is applied to all subsystems from subsystem 3 to subsystem k and this set of equation can be obtained:

$$\begin{bmatrix} 1 & 0 & \cdots & 0 \\ 0 & 1 & 0 & 0 \\ \vdots & \vdots & \ddots & \vdots \\ 0 & 0 & \cdots & 1 \end{bmatrix} = \begin{bmatrix} \eta_{11}^0 & \eta_{12}^0 & \cdots & \eta_{1n}^0 \\ \eta_{21}^0 & \eta_{22}^0 & \cdots & \vdots \\ \vdots & \vdots & \ddots & \vdots \\ \eta_{k1}^0 & \cdots & \cdots & \eta_{kn}^0 \end{bmatrix} \begin{bmatrix} E_{11}^n & E_{12}^n & \cdots & E_{1n}^n \\ E_{21}^n & E_{22}^n & \cdots & E_{2n}^n \\ \vdots & \vdots & \ddots & \vdots \\ E_{k1}^n & \cdots & \cdots & E_{kn}^n \end{bmatrix}. \quad (2.38)$$

4) SEA matrix can be obtained by taking inverse of normalized energy matrix. CLF and DLF can be found by rearranging SEA matrix as:

$$\begin{cases} \eta_{ij} = -\eta_{ji}^0, & i \neq j \\ \eta_{ii} = \sum_{k=1}^n \eta_{ki}^0 \end{cases}. \quad (2.39)$$

If there is a single subsystem DLF can be obtained with PIM since there is no coupling to other subsystems. In this case,

$$\eta = \frac{P_{in}}{\omega E_{tot}}, \quad (2.40)$$

where, $E_{tot} = m \langle v^2 \rangle$ is energy of vibrating subsystem, m is subsystem mass, $\langle v^2 \rangle$ is spatial mean square velocity of subsystem, P_{in} is power input. Power input for each individual frequency is stated as (Lyon & DeJong, 1998):

$$P_{in} = \frac{1}{2} F^2 \operatorname{Re}\{Y_0\}. \quad (2.41)$$

In Equation (2.41), $\operatorname{Re}(Y_0)$ shows the real part of excitation point mobility, F is excitation force. Accordingly, Equation (2.41) can be obtained by substituting Equation (2.41) to Equation (2.40).

$$\eta = \frac{\operatorname{Re}\{Y_0\}}{\frac{2\omega}{N} \sum_{i=1}^N |Y_i^2|}, \quad (2.42)$$

Here, N is the number of measurement point. In this method spatial averaging of subsystem energy is necessary. In the case of trying to find broad band DLF, implementing the same procedure on multiple excitation points gives more accurate results. As a result of power injection method that is based on SEA, the results are more accurate at high frequency region of the subsystems.

2.4 Monte Carlo Simulation

Monte Carlo method is relying on random sampling to obtain numerical results. It is generally used in engineering problems especially when it is difficult or impossible to use other mathematical methods. Monte Carlo method is mainly used in optimization, numerical integration with a probability distribution. It is efficiently used in many different areas such as statistical stock exchange modeling, weather, earthquake forecasting, and dynamic analyses of uncertain systems. This method is based on an estimation of outputs with specified input functions which are modeled as particular distribution functions like Gaussian, Rayleigh distribution, etc..

For uncertainty analyses, Monte Carlo simulation is especially used together with low frequency deterministic techniques such as FEM, BEM. However, using these techniques at mid and high frequency region on uncertain systems, especially for the structures having over one million degree of freedoms (DOF) leads to at least tenfold increase on solution time.

CHAPTER THREE MODAL ANALYSIS

In this chapter, modal analyses of an aluminum hollow beam, a single composite plate and a T-type composite structure are performed. Here, only for the single plate, a mathematical model is constructed. For the other structures except beam, natural frequencies are numerically and experimentally obtained. The details of measurement setup are given in Appendix A. It is noted that the numerical analyses results were taken from (Tübitak Project Report, 112M836, 2015) and used for comparison here in this chapter. Modal analysis was made only experimentally for the beam in order to determine the modal behavior of the simple structure.

3.1 Modal Analysis of a Beam

In this part of the study, modal analysis was implemented to a 50x50x2 aluminum hollow beam (Figure 3.1). Mechanical properties of the beam are given in Table 3.1.



Figure 3.1 Aluminum hollow beam

Table 3.1 Mechanical properties of the beam

Property name	Beam
Density [kg / m^3]	2700
Modulus of Elasticity [MPa]	69000
Poisson ratio	0.33
External dimensions [m x m x m]	1 x 50e-3 x 50e-3
Internal dimensions [m x m x m]	1 x 46e-3 x 46e-3
Structural damping (η)	0.0168

In order to maintain free boundary condition in experimental analyses, beam was hanged from two ends with flexible strings. Input excitation was provided with impact hammer. In Figure 3.1, all three labeled points are used for both response and excitation.

The beam was tested with Native Instruments Signal Express software. Selected three points on the beam were excited and measured in order. Verification of the experimental analysis can be examined in Figure 3.2 via symmetry test and anti node tracing. Here the spectra are given in terms of accelerance which is the ratio of acceleration to the force. Responses from the same excitation and response points are reciprocally similar which shows that the analyses have been made properly.

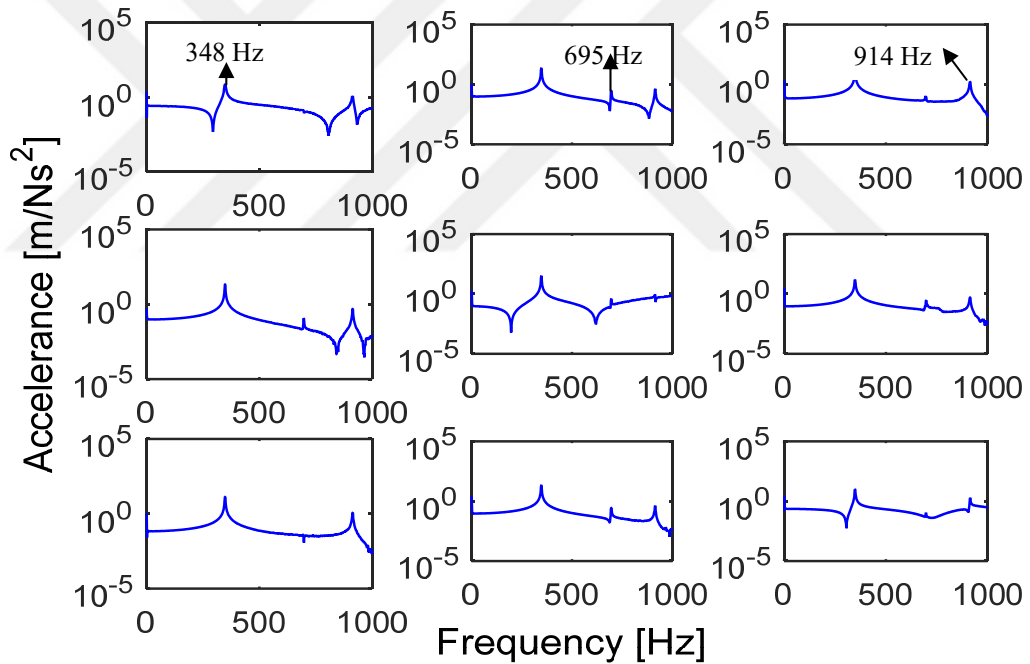


Figure 3.2 Accelerance response of the aluminum hollow beam with predicted natural frequencies

3.2 Modal Analysis of a Composite Plate

Modal analysis of 8-layered symmetric composite plate was performed experimentally and numerically in this chapter of the study. Experimental modal analysis was performed for the composite plate in order to obtain low-frequency

modal parameters. In experimental modal analysis SDOF approach (Peak selection) method was used.

3.2.1 The Composite Plate

Here, dynamic analysis of a composite plate shown in Figure 3.3, was performed.

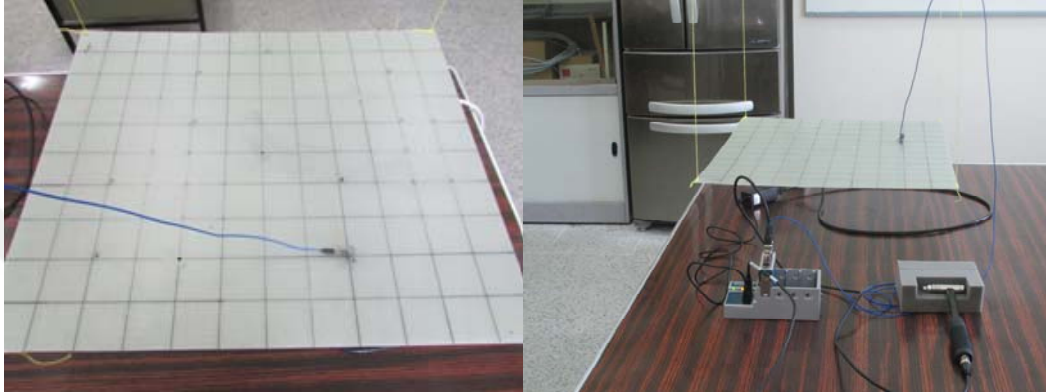


Figure 3.3 Experimental modal analysis setup

The glassfibre epoxy plate was produced in Dokuz Eylül University Composite Manufacturing Laboratory as having (0-90-0-90-90-0-90-0) orientation angles. Physical and mechanical properties of the plate are tabulated in Table 3.2. The plate contains glass fibers and epoxy resin.

Table 3.2 Mechanical and physical properties of plate

Property	Value
Length along direction of x [m]	0.5
Length along direction of y [m]	0.6
Thickness [m]	2.50E-03
Young modulus along direction of x [GPa]	21.3
Young modulus along direction of y [GPa]	21.1
Shear modulus along direction of x [MPa]	3003
Poisson ratio along direction of x (ν_{12})	0.161

3.2.2 Experimental Modal Analysis

The composite plate with the setup is shown in Figure 3.3. The plate was excited from its eight different points with an impact hammer. Vibration receptance frequency responses were obtained from the same points. Reliability of the modal analysis can be examined in Figure 3.4.

In Figure 3.4, symmetric responses from the same excitation and response points are reciprocally similar, which show that analyses have been made properly.

Natural frequencies, damping ratios and modal constants can be derived from one of the receptance results by using peak selection method as given in Section 2.1.1. The modal parameters are indicated in Table 3.3.

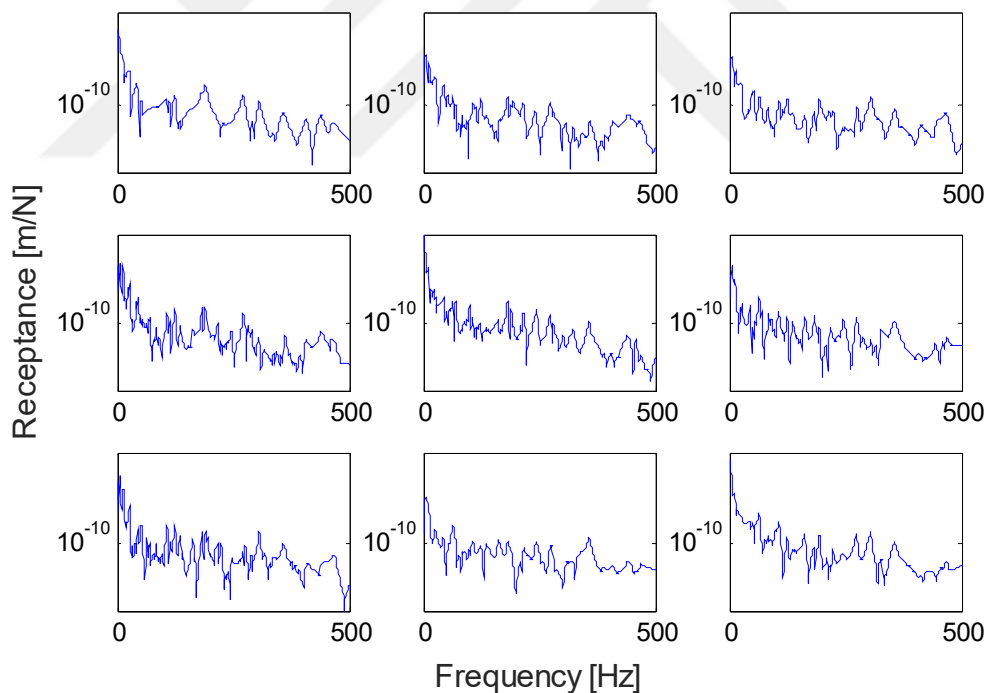


Figure 3.4 Modal analysis results of the composite plate

Table 3.3 Natural frequencies, damping ratios, modal constants of the composite plate

Numerical Natural Frequencies [Hz]	Experimental Modal Analysis			
	\bar{f}_n [Hz]	$\bar{\zeta}_n$	\bar{A}_n	$\bar{\alpha}_{n,\max}$ [m/N]
10.206	12.4	0.093	2.282	0.00236
21.647	21.5	0.055	0.852	0.000629
30.082	27.3	0.047	0.713	0.000303
31.782	32	0.047	0.237	6.76E-05
37.562	37	0.038	0.204	5.33E-05

The mathematical five-DOF model of frequency response function of the plate can be written by using parameters obtained from first five modes, as

$$\begin{aligned}
 \alpha(\omega) &= \sum_{n=1}^5 \frac{A_n}{\omega_n^2 - \omega^2 + 2j\omega\omega_n\eta_n} \\
 &= \frac{2.282}{(2\pi 12.4)^2 - \omega^2 + 2j\omega(2\pi 12.4)(2 \cdot 0.093)} \\
 &\quad + \frac{0.852}{(2\pi 21.5)^2 - \omega^2 + 2j\omega(2\pi 21.5)(2 \cdot 0.055)} \\
 &\quad + \frac{0.713}{(2\pi 27.3)^2 - \omega^2 + 2j\omega(2\pi 27.5)(2 \cdot 0.047)} \\
 &\quad + \frac{0.237}{(2\pi 32)^2 - \omega^2 + 2j\omega(2\pi 32)(2 \cdot 0.047)} \\
 &\quad + \frac{0.204}{(2\pi 37)^2 - \omega^2 + 2j\omega(2\pi 37)(2 \cdot 0.038)}
 \end{aligned} \tag{3.1}$$

and it is displayed in Figure 3.5.

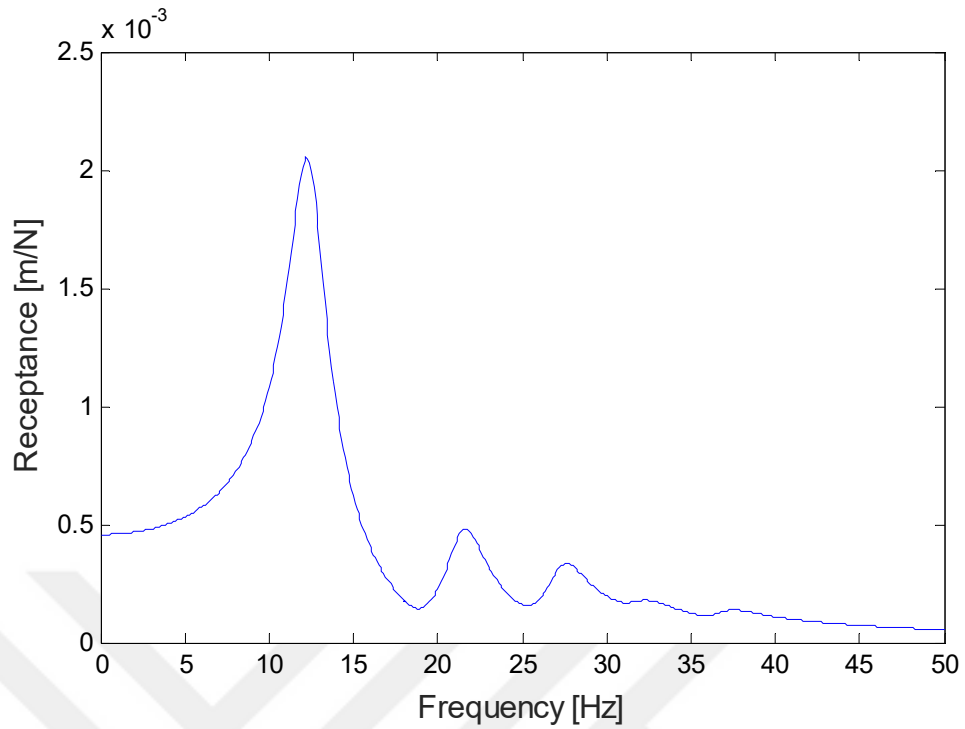


Figure 3.5 Frequency response function of the five-DOF composite plate model

3.3 Modal Analysis of a T-type Structure

In this part of the study, numerical and experimental modal analyses are performed for a T-type structure as shown in Figure 3.6. The structure consists of three composite plates having the same mechanical properties with the previous plate and three corner irons. The structure was hanged with flexible string in order to maintain free boundary condition as shown in Figure 3.6.



Figure 3.6 T-type structure with point connections

3.3.1 Numerical Modal Analysis

As it is mentioned before all numerical results are taken from (Tübitak Project Report, 112M836, 2015). The structure was modeled by ANSYS APDL and ANSYS Workbench and is given in Figure 3.7. Predicted natural frequencies are tabulated in Table 3.4.

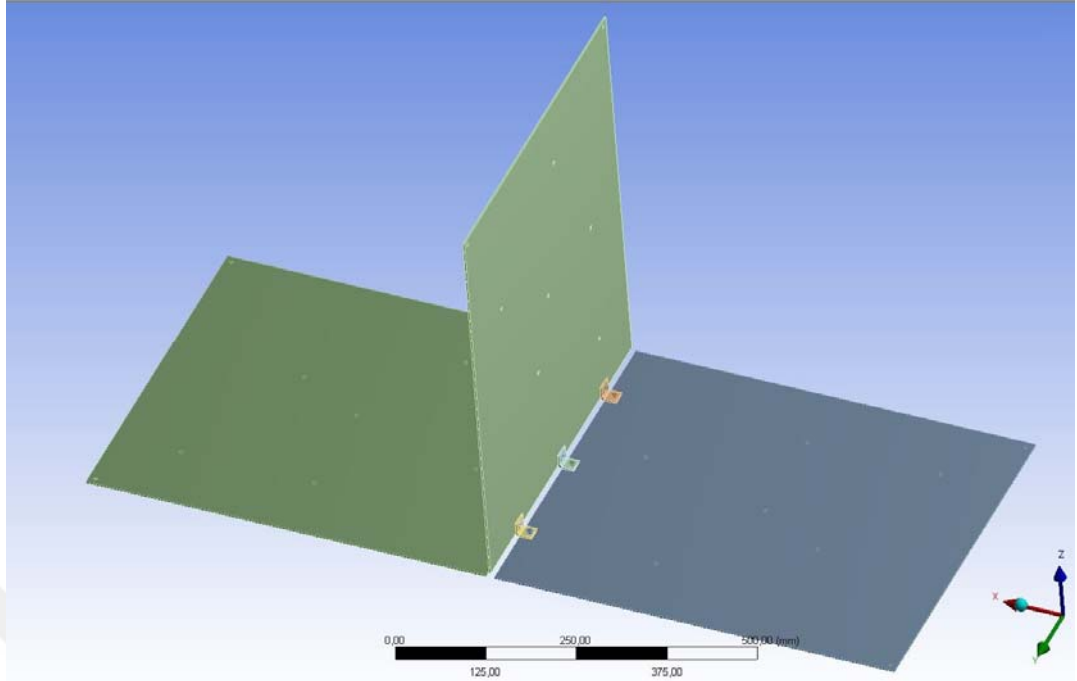


Figure 3.7 Numerical model of the T-type structure (Tübitak Project Report, 112M836, 2015)

3.3.2 Experimental Modal Analysis

Here the T-type complex structure shown in Figure 3.6 was excited from randomly selected two points of each plate, and vibration responses were measured from these points. The measurement setup is shown in Figure 3.8. Here, receptance response, which is the ratio of vibration velocity over force, was measured for each excitation.

The label “*zimojn*” at Figure 3.9 indicates that excitation is applied at n th point of i th plate and measurements are taken from m th point of j th plate. Note that, here, when $im = jn$ is called as driving point whereas $im \neq jn$ denotes transfer receptances.

Receptance responses are given in Figure 3.9. Symmetry test and anti node observation state the accuracy of the measurements. Natural frequencies obtained from peak selection method are compared with those of numerical predictions in Table 3.4. It is shown that natural frequencies predicted by experiments are very consistent with those predicted by finite element method.

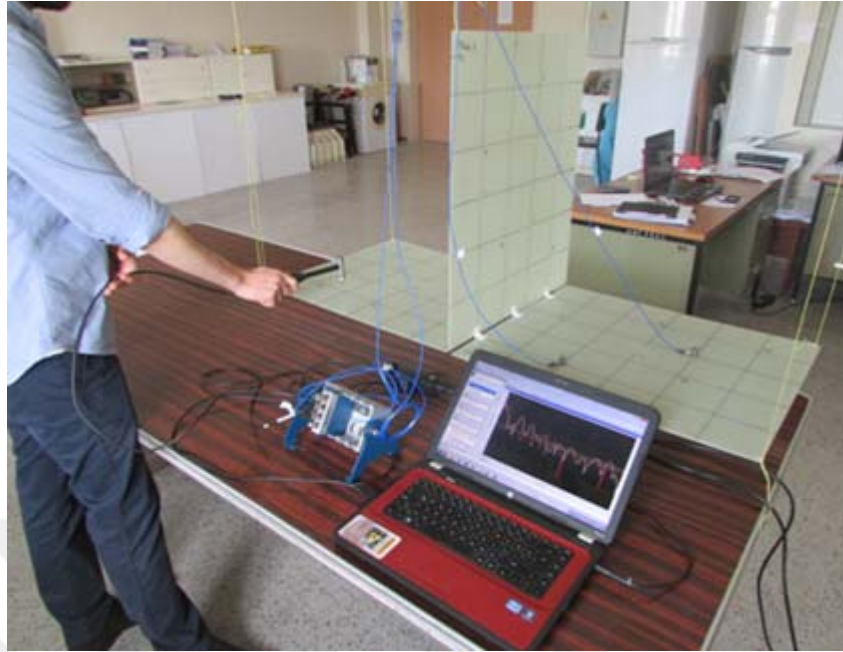
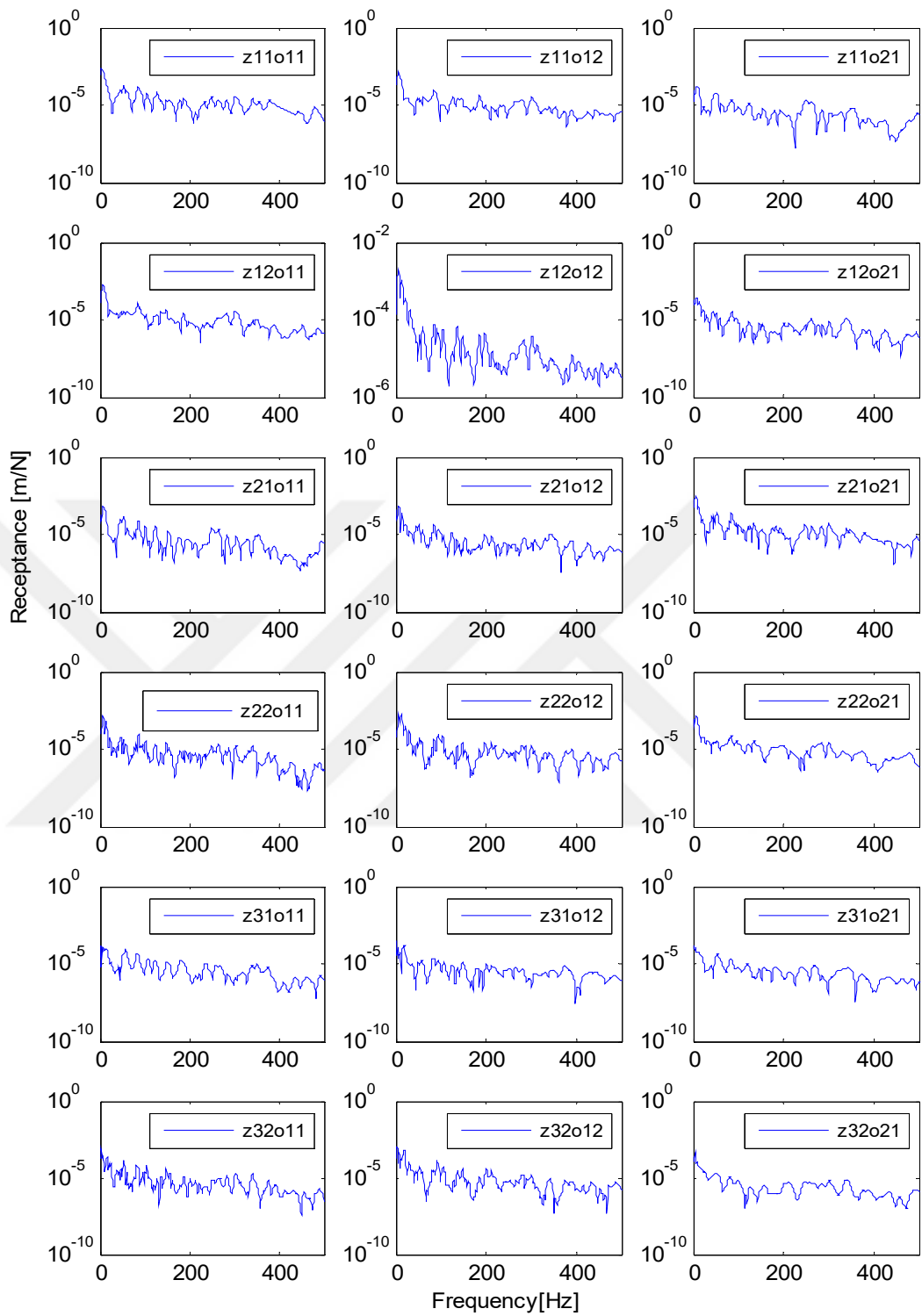
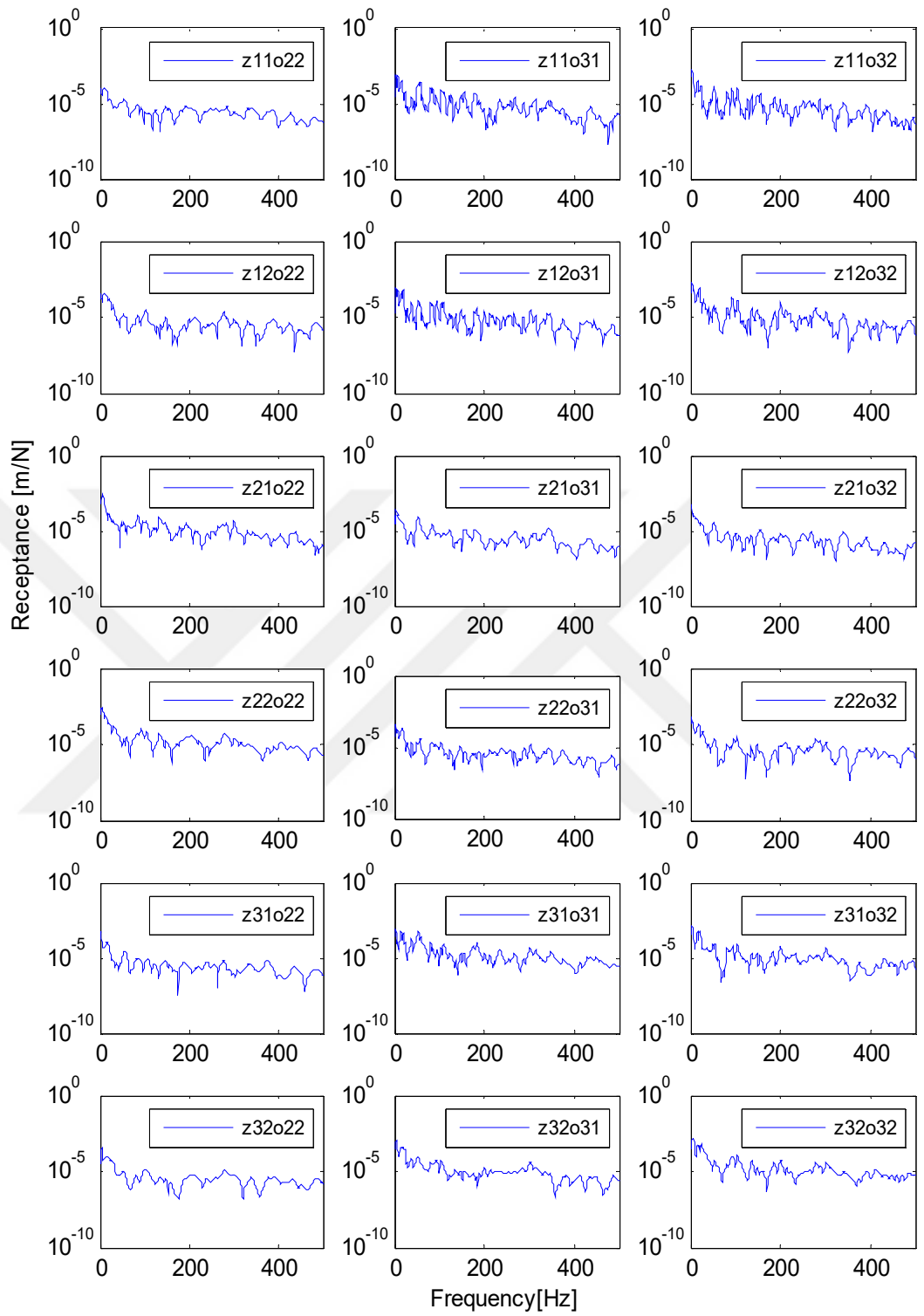


Figure 3.8 Experimental modal analysis setup of the T-type structure



a)

Figure 3.9 Transfer receptances of composite structure a) first half, b) second half



b)

Figure 3.9 Transfer receptances of composite structure a) first half, b) second half (continued)

Table 3.4 Experimental and numerical (Tübitak Project Report, 112M836, 2015) natural frequencies obtained from Peak Selection Method

Mode Number	Frequency [Hz]	
	Experimental	Numerical
1	3	3.6254
2	4	4.2689
3	5	5.1924
4	6	6.7058
5	7	7.2539
6	14	14.7940
7	21	21.5140
8	21	21.5910
9	23	23.2420
10	25	26.2050
11	25	26.5150
12	33	33.1800
13	33	33.6240
14	33	33.6310
15	46	46.4380
16	48	48.6560
17	48	49.3550
18	48	49.3780
19	53	53.3610
20	60	60.2970

CHAPTER FOUR

DETERMINATION OF SEA PARAMETERS OF STRUCTURES

For the high frequency analyses purpose, SEA, a very common method was considered in the study. Here it is necessary to determine SEA parameters such as coupling loss factor (CLF) and damping loss factor (DLF) of subsystems. In the determinations, Power Injection Method (PIM) as given in Section 2.3 was used.

Here, only DLFs of aluminum hollow beam and single plate were obtained since there is no coupling with other structures. However, for I-, L- and T-type structures, CLFs and DLFs were predicted. The details of measurement setup are given in Appendix B. It is noted that the numerical analyses and analytical results were taken from (Tübitak Project Report, 112M836, 2015) and used for comparison here in this chapter.

4.1 Determination of the DLF of an Aluminum Beam

Here, experimental Power Injection Method (PIM) is applied. An aluminum beam was excited via a vibration exciter from its randomly selected three points as shown in Figure 4.1 and total energies were measured from its randomly selected seven points but including those three driving points. Then energies are spatially averaged to present the single energy level of the beam.



Figure 4.1 Aluminum hollow beam

Calculated damping loss factor (DLF) was averaged over 1/3 octave band of each single frequency and shown in Figure 4.2. Averaged damping throughout the entire spectrum is calculated as 0.0198.

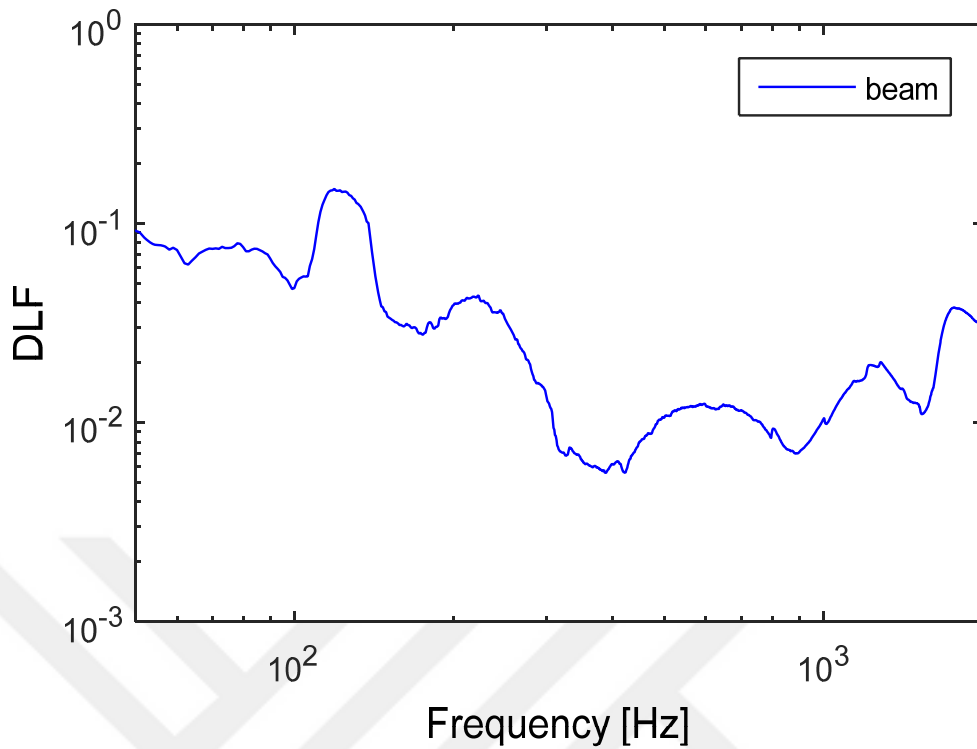


Figure 4.2 Damping loss factor of the beam

4.2 Determination of the DLF of a Single Composite Plate

Here, experimental setup for Power Injection Method (PIM) is shown in Figure 4.3a. A single composite plate was excited from its three different points, as shown in Figure 4.3b, and energy measurements were taken from randomly selected eight different points but including those three driving points. Then energies of these eight points are spatially averaged to present the single energy level of the plate. The plate is the same plate which is considered in the previous analyses.

1/3 octave band averaged DLF results are given in Figure 4.4. Approximate high frequency threshold of this plate is calculated in terms of MOF as given in Section 2.2.2. The threshold is found as 630 Hz when MOF equals to 2.5 for plates.

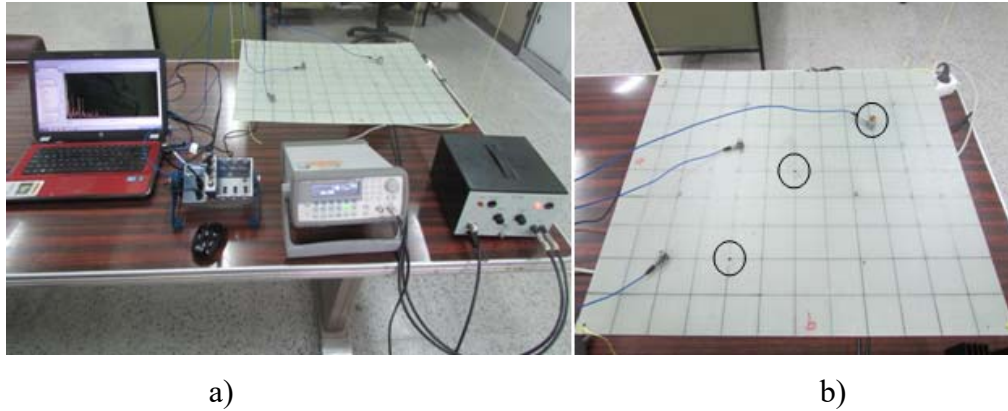


Figure 4.3 Experimental setup for the determination of damping loss factor

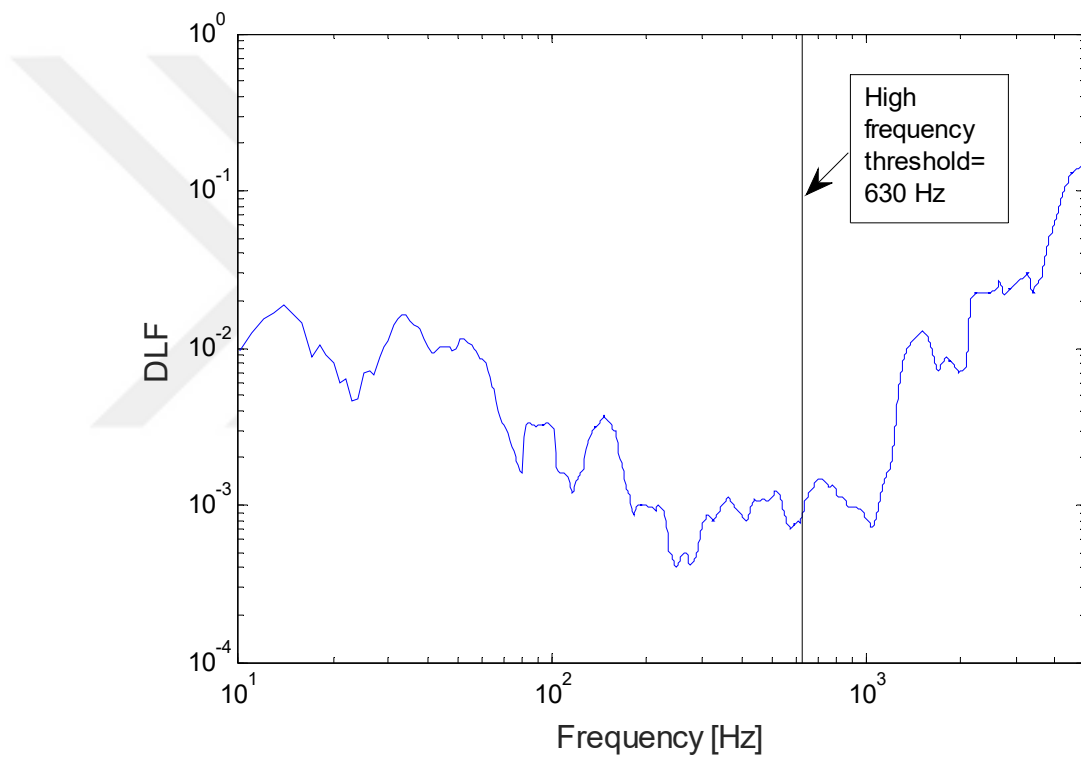


Figure 4.4 Damping loss factor of the plate

4.3 Calculation of SEA Parameters of I-, L-, T- Type Structures

Here, experimental and numerical PIM was implemented to I-, L-, T-type structures with point connections as schematically given in Figure 4.5 in order to obtain SEA parameters.

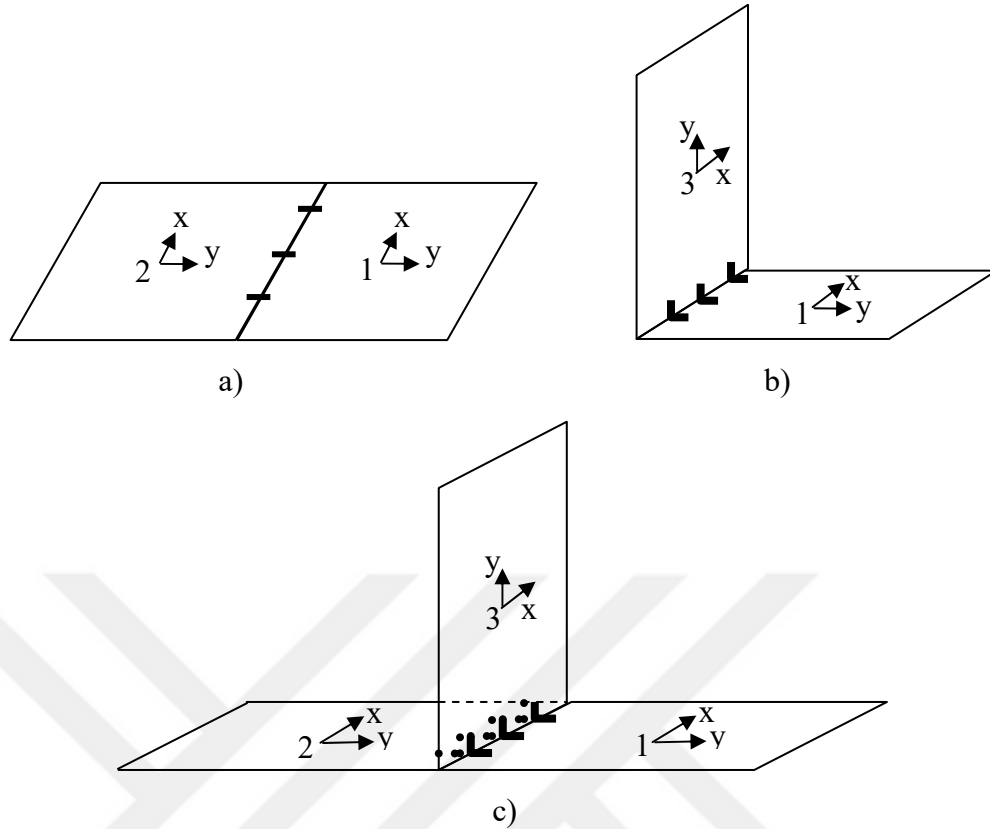


Figure 4.5 Composite structures a) I-type, b) L-type, c) T-type

Experimental PIM measurement setup is given in Figure 4.6. All structures were hanged by flexible strings in order to provide free boundary condition. Power injection was then applied to the plates as broadband noise by a vibration exciter, and finally mobility responses were measured from these plates. Here, for each plate, their two points were excited and twenty points were measured with including excitation points.

In numerical PIM analysis, for each plate, again their two points were excited however, in this time, two-hundred measurement points are considered to contribute to single energy levels for each individual plate by spatial averaging. Computed loss factors of the I-, L- and T-type structures are presented in Figures 4.7-4.9, respectively. Besides that, analytical CLFs computed by infinite impedances of substructures are also given as comparison. DLFs of structures are also compared with those of single plate which was studied in the previous section.



Figure 4.6 Experimental setup for power injection method,

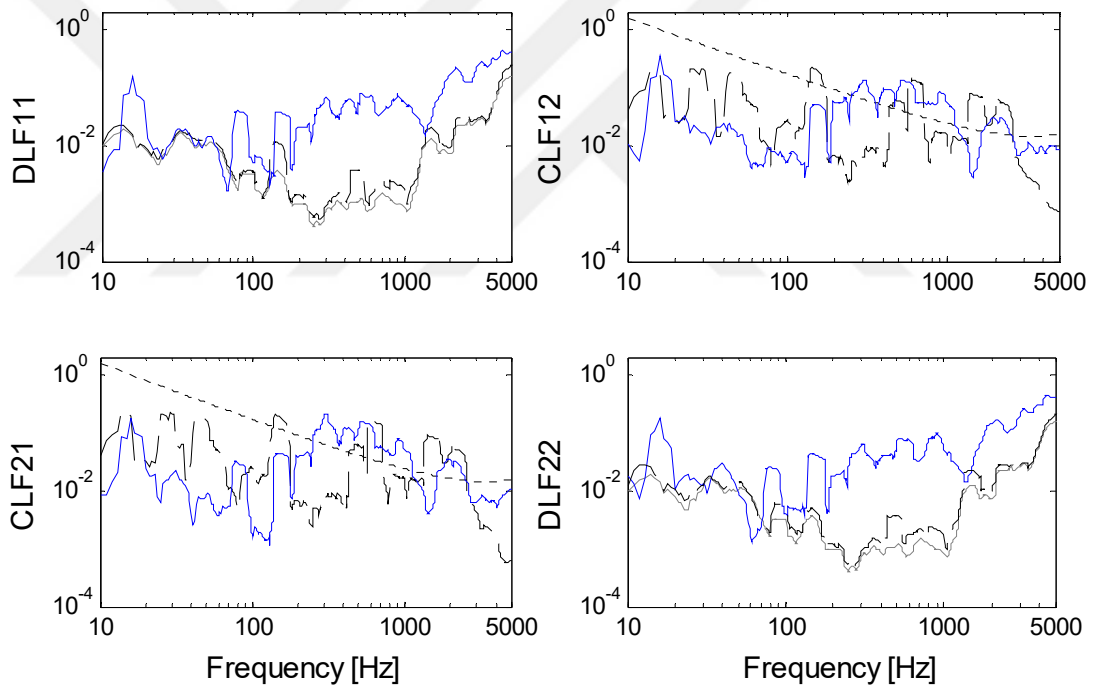


Figure 4.7 Loss factors of I-type composite structure (blue line: experimental, dashed: numerical (Tübitak Project Report, 112M836, 2015), grey: single plate (from Figure 4.4), dotted: SEA (Tübitak Project Report, 112M836, 2015))

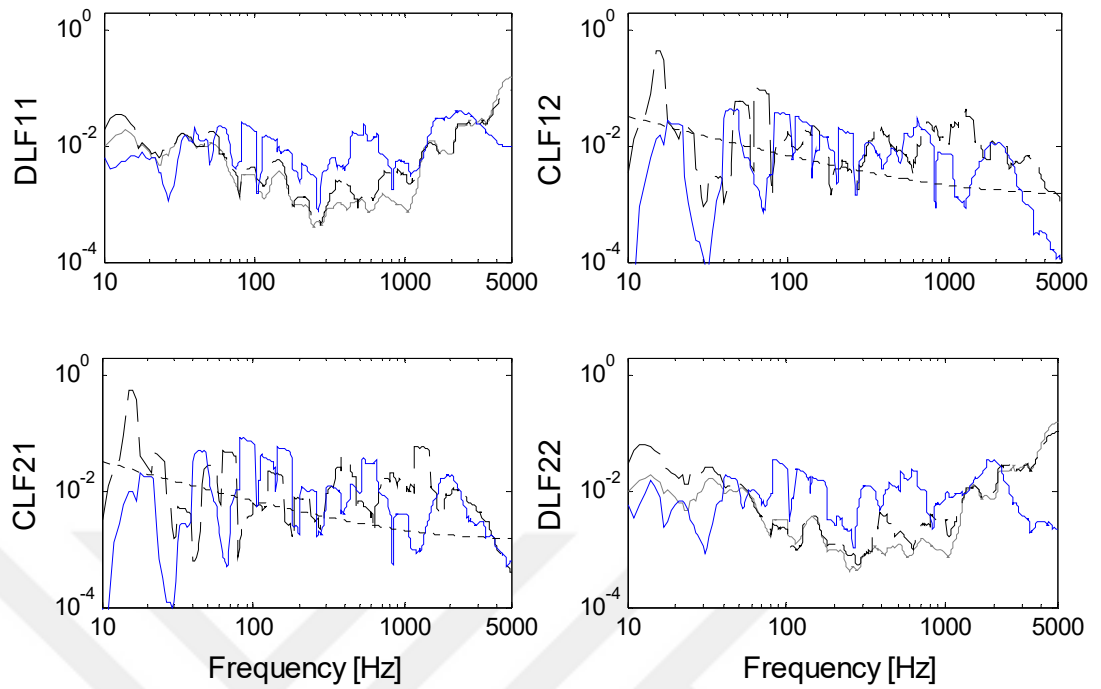


Figure 4.8 Loss factors of L-type composite structure (blue line: experimental, dashed: numerical (Tübitak Project Report, 112M836, 2015), grey: single plate (from Figure 4.4), dotted: SEA (Tübitak Project Report, 112M836, 2015))

As seen in Figures 4.7-4.9, DLF results of composite plate in I-, L-, T-type structures are coherent with single plate results in lower frequencies. However, it is observed that considerable discrepancies exist by increasing frequency. This is probably caused by the indirect coupling of each plates.

As far as CLFs are considered, although relatively small discrepancies exist, especially for higher frequencies, very good correlation was obtained.

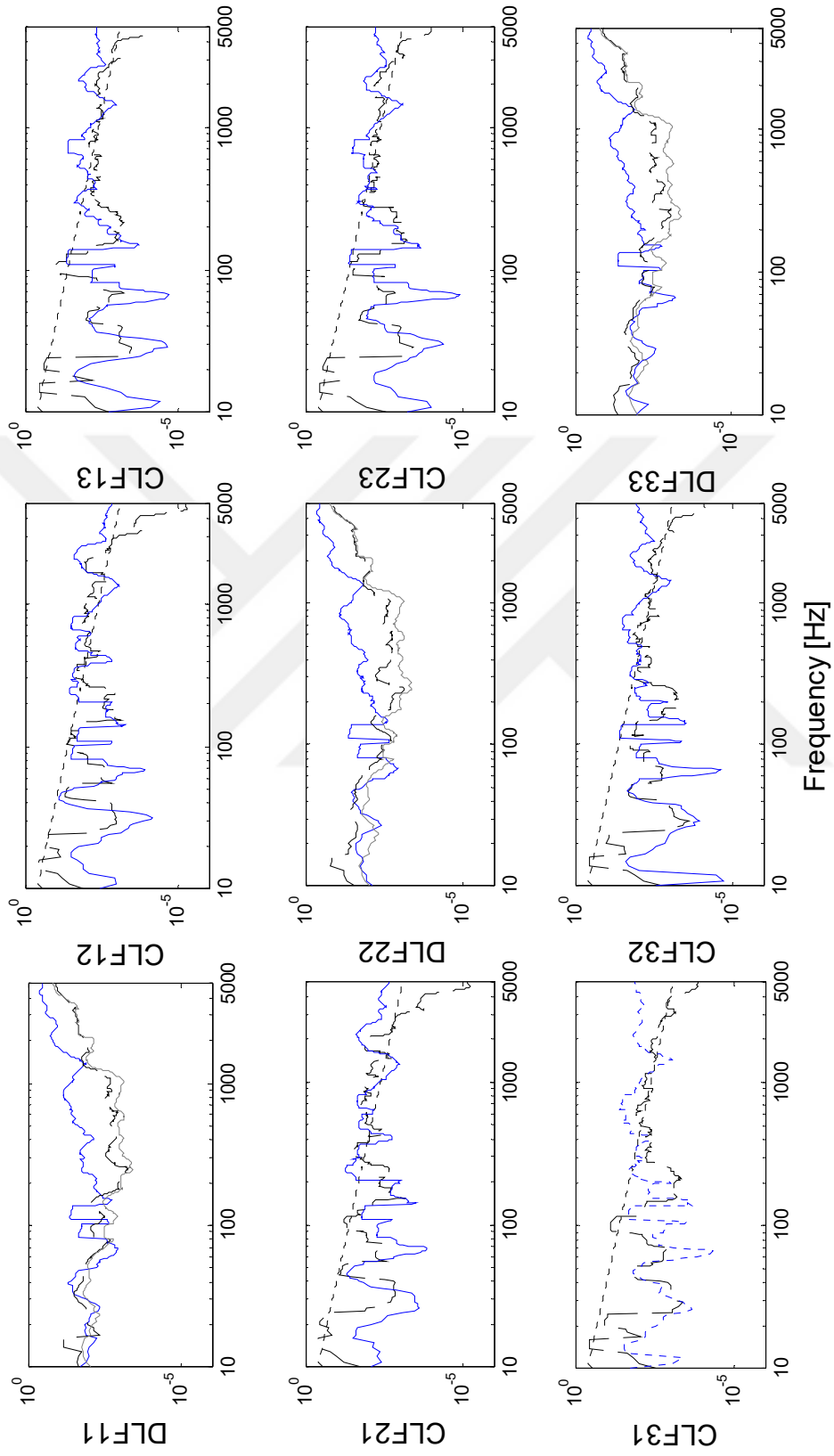


Figure 4.9 Loss factors of T-type composite structure (blue line: experimental, dashed: numerical (Tübitak Project Report, 112M836, 2015), grey: single plate (from Figure 4.4), dotted: SEA (Tübitak Project Report, 112M836, 2015))

CHAPTER FIVE UNCERTAINTY ANALYSES OF COMPOSITE STRUCTURES

In this chapter, uncertainty analyses were made for several structures from simple to complicated ones. Table 5.1 shows a brief representation of the analyses performed in the study. The details of measurement setup are given in Appendix C. It is noted that the numerical analyses results were taken from (Tübitak Project Report, 112M836, 2015) and used for comparison here in this chapter.

5.1 Uncertainty Analysis of A Single Composite Plate

In this part of the study, numerical and experimental uncertainty analyses were performed. The effect of the uncertainty on the natural frequency and vibration response are examined. For the effect of uncertainty on the natural frequencies, numerical Monte Carlo simulation was performed for thickness uncertainty.

The change in the mass of the plate was chosen as an uncertainty parameter in numerical and experimental analyses. It is altered by random normal (Gaussian) distribution with 5% of standard deviation. During analyses plate was excited from its three different points as shown in Figure 5.1.

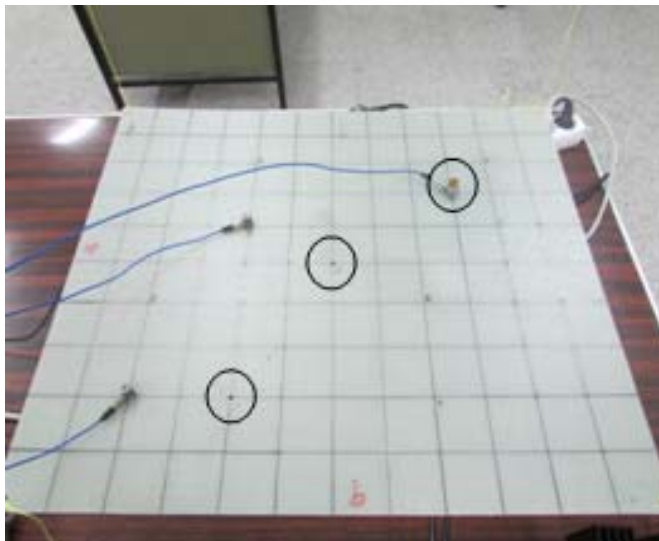


Figure 5.1 Driving points of the plate

Table 5.1 Brief of analyses made in the chapter

STRUCTURE	Analysis Type	Uncertainty parameter			Effect of Uncertainty	
		Mass of plate	Center of gravity		On natural frequency	On frequency spectrum
		Simulation parameter				
	Adding small masses	Changing thickness	Changing location of small masses			
Single composite plate	Experimental	x		x		x
	Numerical		x		x	x
T-type composite structure	Experimental	x		x		x
	Numerical		x			x
Stiffened composite plate	Experimental	x		x		x
	Numerical		x			x
Composite Cabinet	Experimental	x		x		x
	Numerical		x			x

5.1.1 Effect of Uncertainty on Natural Frequencies

Here, numerical analyses were implemented for random distribution of the plate thickness with 5% standard deviation to represent the mass variability. 100 samples of plate thicknesses are given in Figure 5.2. Numerical Monte Carlo simulation of natural frequencies at first 150 modes was obtained. The results are presented in Figure 5.3.

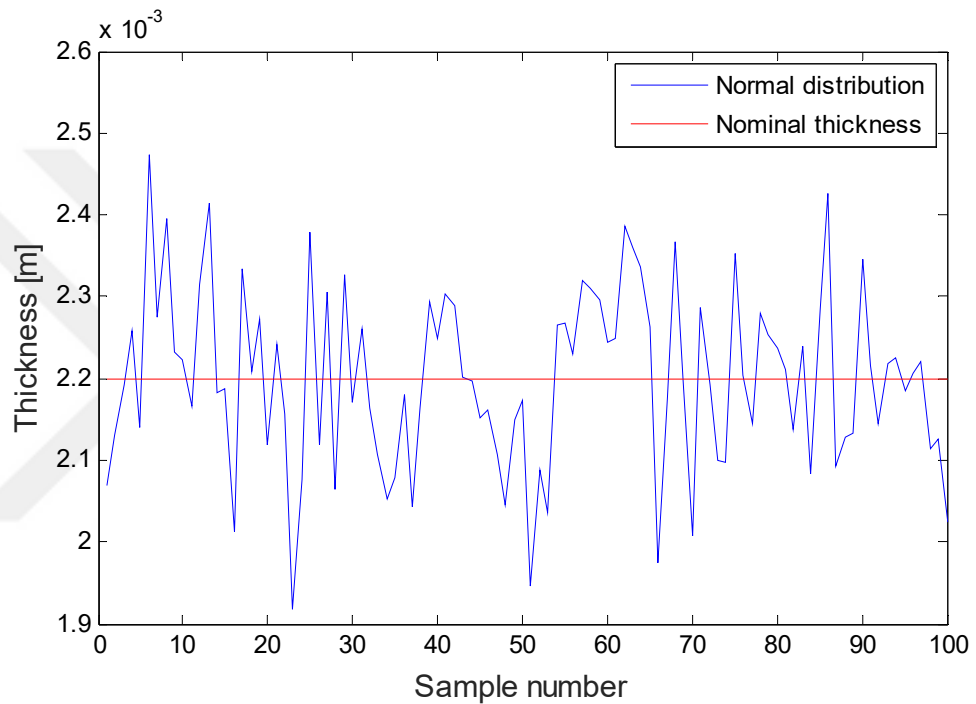


Figure 5.2 Thickness samples of the plate (Tübitak Project Report, 112M836, 2015)

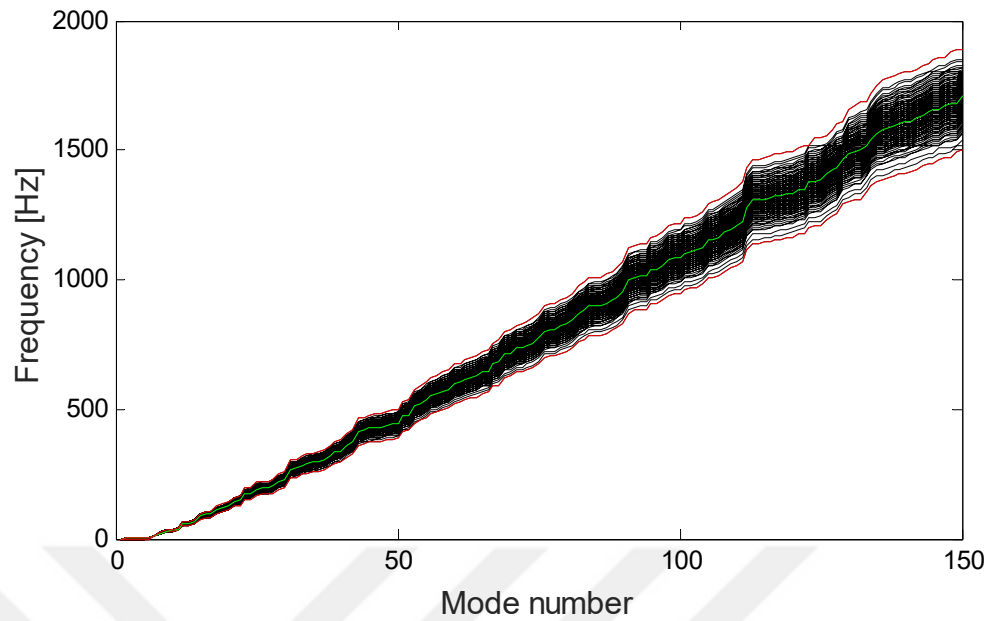


Figure 5.3 Uncertainty effect on natural frequencies (Tübitak Project Report, 112M836, 2015)

The results clearly show that the uncertainty effects on natural frequencies considerably increases at higher modes. This states that for reliable analyses uncertainty effect should be taken into consideration, especially for mid and high frequency analyses.

5.1.2 Effect of Uncertainty on Frequency Response Function

Experimental Monte Carlo simulations were performed here in this part of the study for the effect of uncertainty on the frequency response function. Plate mass variability was selected as uncertainty parameter; however, in this case, several small masses are used to simulate the mass variability for simplicity. In this regard, as shown in Figure 5.4, 20 small masses (not exceeding 5% of the total mass of the plate) were attached on the plate.

The composite plate was hanged by flexible strings to provide free boundary condition and excited from its three different points as shown in Figure 5.5 and 5.4, respectively. Here it is also small mass distribution and measurement points were altered randomly in each measurement. In total, sixty measurements (twenty points corresponding to three different excitation points) were performed.

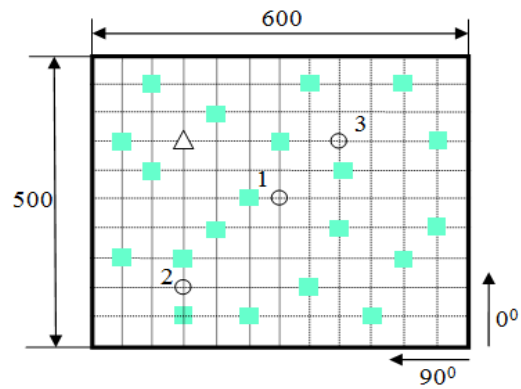


Figure 5.4 Schematic representation of driving points and locations of added masses (o: driving points, Δ : randomly located measurement points)



Figure 5.5 Experimental setup of uncertainty analysis

Driving point mobilities and transfer mobilities of 60 experiments are shown in Figure 5.6. and 5.7, respectively.

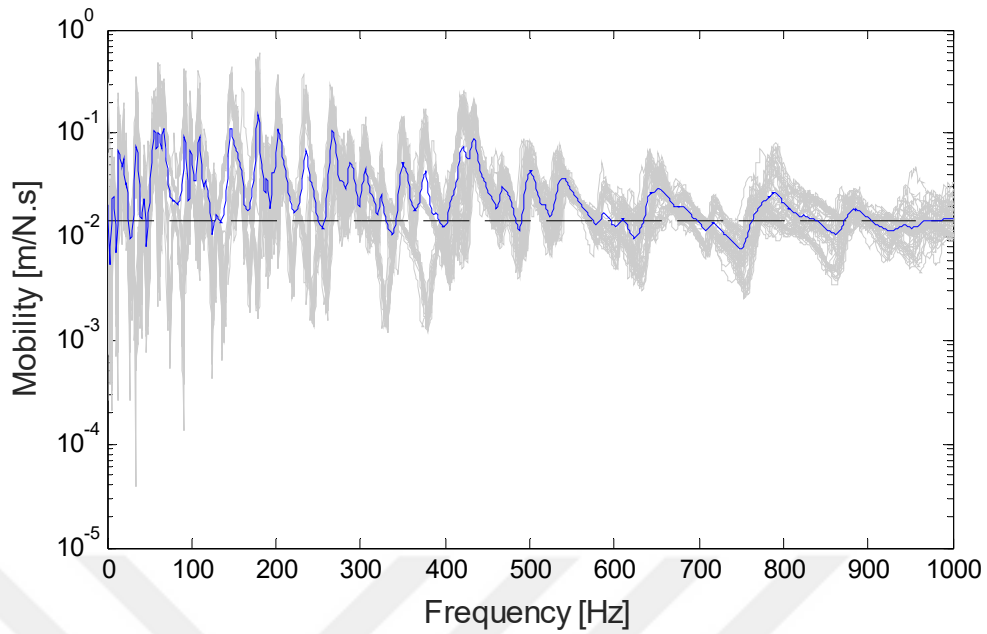


Figure 5.6 Experimental driving points mobilities of the plate (grey: uncertain result of 60; dashed dot: mean experimental result of driving points; dashed line: infinite system mobility (Tübitak Project Report, 112M836, 2015))

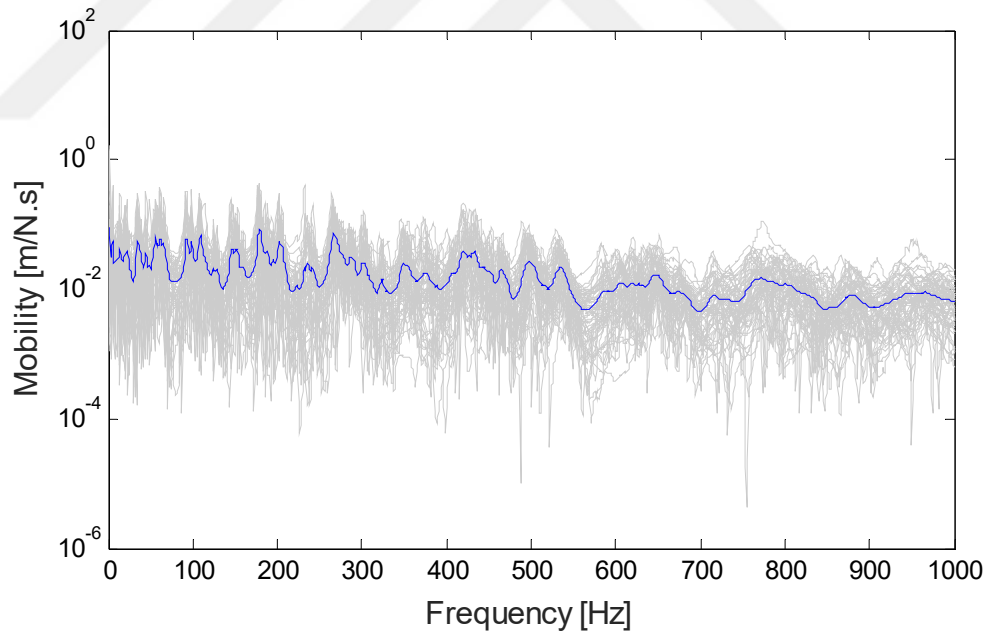


Figure 5.7 Experimental transfer mobilities of the plate (grey: uncertain result of 60; dashed dot: mean experimental result of transfer points)

Figure 5.6 also indicates analytical (infinite) mobility of the orthotropic plate. It is noted that analytical expression that given in Chapter 2.2.1.3 about infinite system mobility is valid only for high frequency region because of its theoretical limitations.

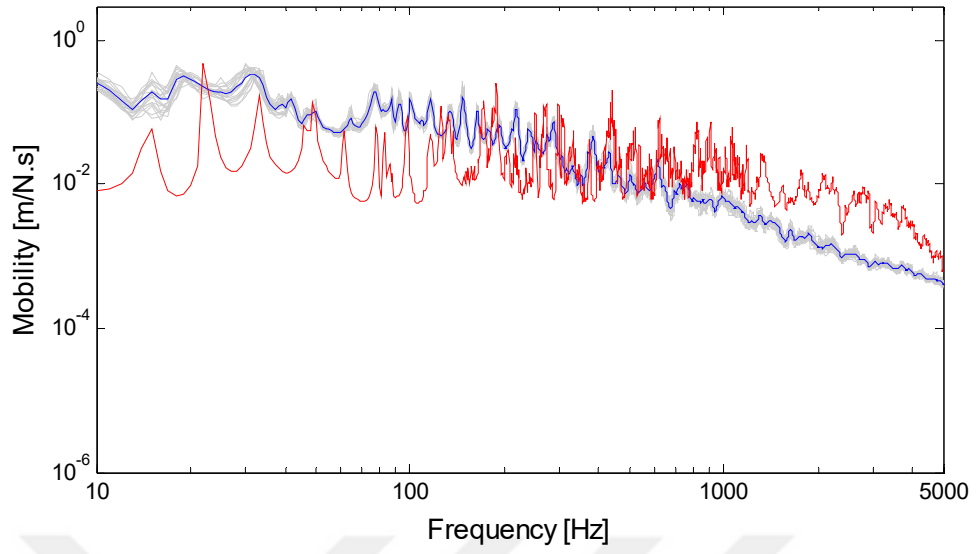
The harmony of measurements with the analytical results shows that experiments were accurately made and reliably used in further analyses.

5.2 Uncertainty Analysis of T-type Structure

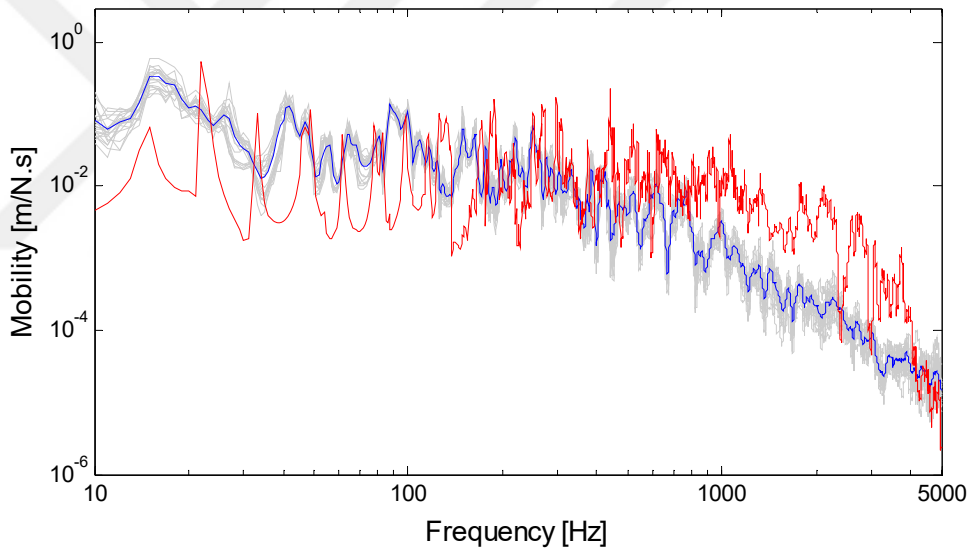
In this section, mass of T-type structure was selected as uncertainty parameter and each plate's mass was altered as doing not to exceed its 5% mass in order to create 20 samples. Here the excitation was applied to only plate 1 shown in Figure 4.5c.

Experimental mobilities of the plates with uncertain results were given together with numerical mean mobilities in Figure 5.8. Although their simulation parameters are different, since uncertainty parameter (mass) is the same for both numerical and experimental studies, the results can be comparable. It is seen that experimental uncertainty makes small effects in entire spectrum. When comparing with numerical mean predictions, only in a limited range there is consistency between results. The discrepancy in general can be due to the boundary condition inconsistency, however, in higher frequencies, experiments can not be performed successfully due to the fact that excitation power is not enough to excite the higher modes of the system due to its mass.

In Figure 5.9-5.11, mean values of experimental SEA whose parameters are found via PIM, analytical SEA whose parameters are found via infinite system impedances, direct measurements and numerical results are shown for plates 1-3 in Figures 5.9-5.11, respectively.

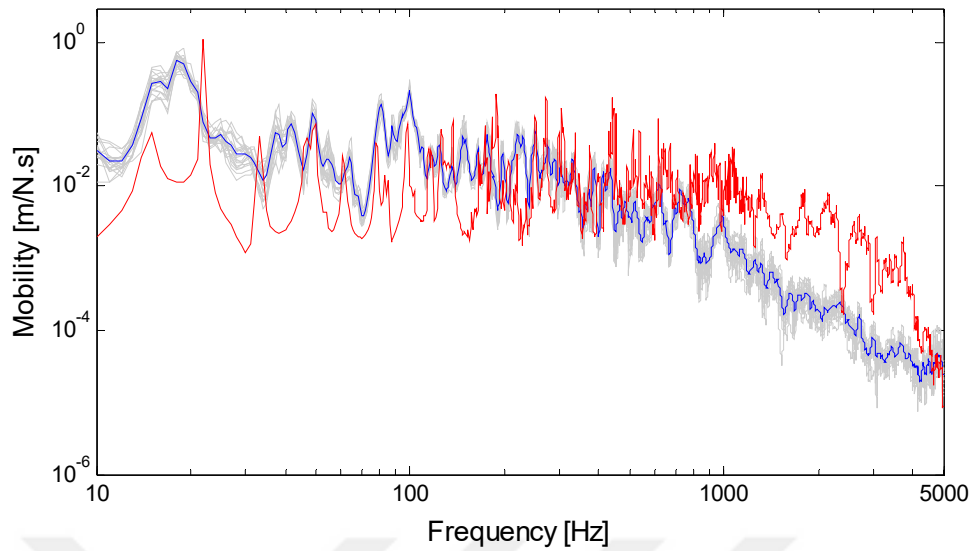


a)



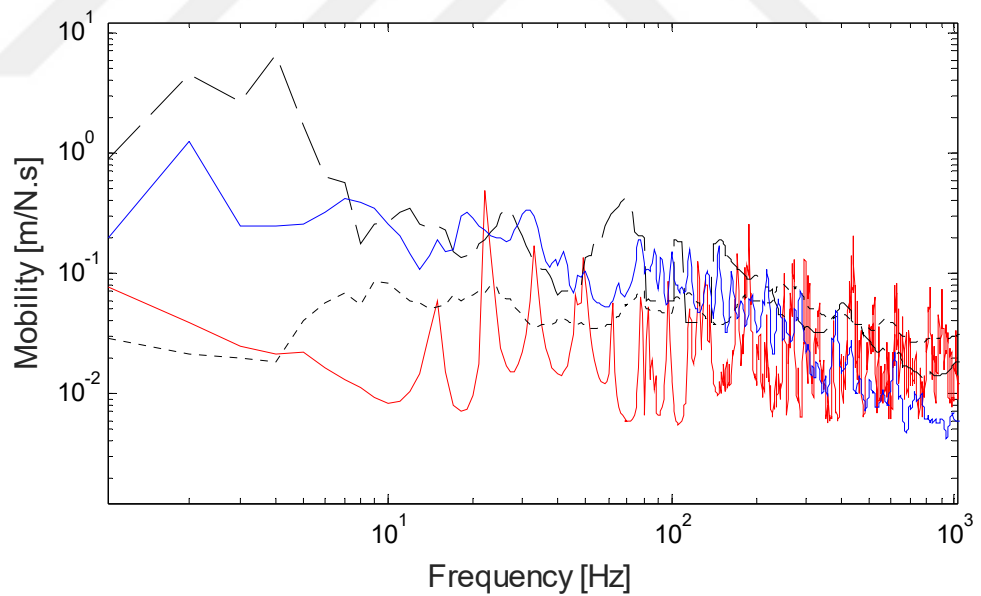
b)

Figure 5.8 Experimental and numerical uncertainty results of T-Type structure a) subsystem 1 b) subsystem 2 c) subsystem 3 (grey: experimental uncertainty results, blue line: mean experimental uncertainty results, red line: mean numerical uncertainty results (Tübitak Project Report, 112M836, 2015))



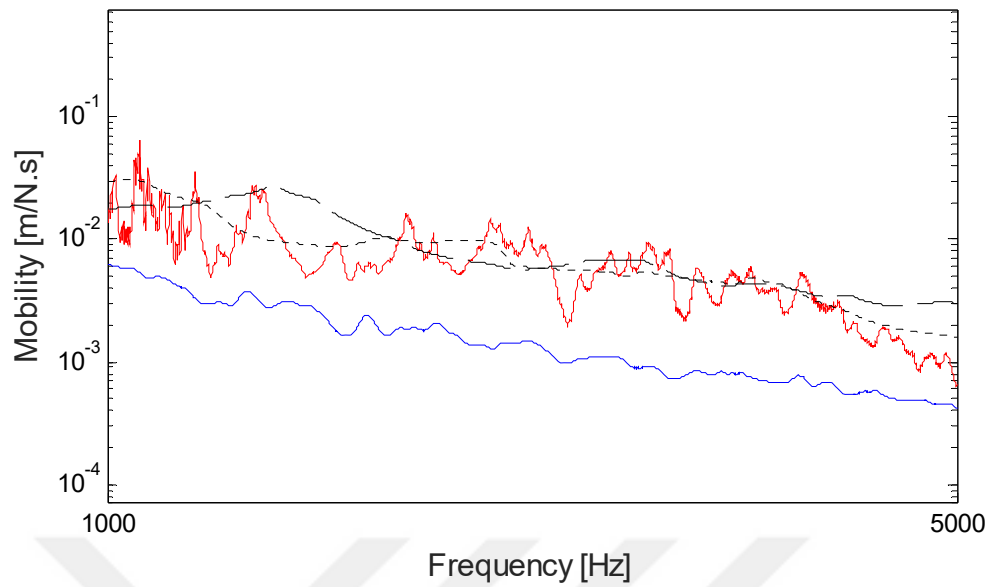
c)

Figure 5.8 Experimental and numerical uncertainty results of T-Type structure a) subsystem 1 b) subsystem 2 c) subsystem 3 (grey: experimental uncertainty results, blue line: mean experimental uncertainty results, red line: mean numerical uncertainty results (Tübitak Project Report, 112M836, 2015)) (continued)



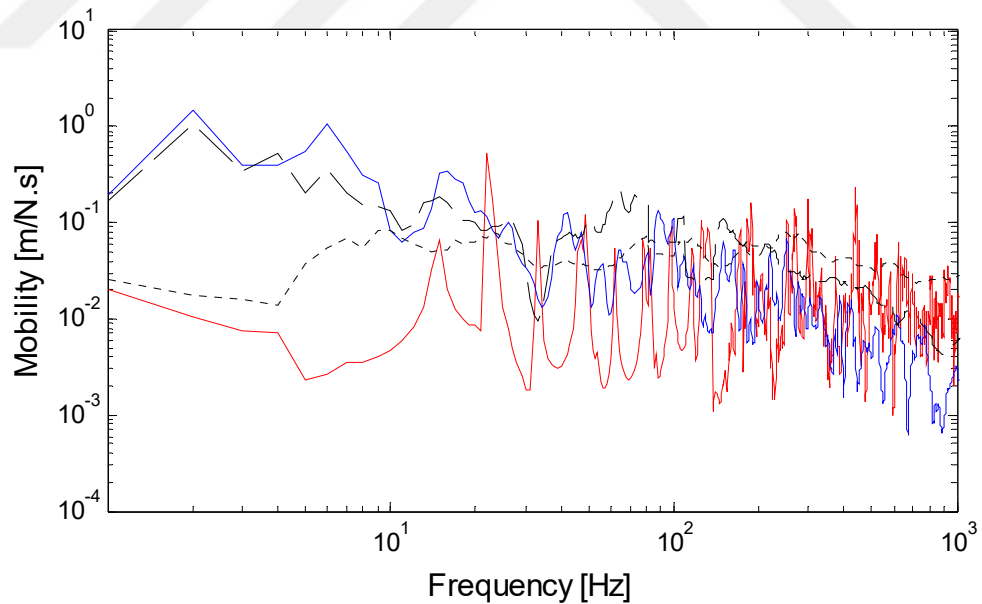
a)

Figure 5.9 Response comparison of subsystem 1 in T-type structure a) 10-1000 Hz, b) 1000-5000 Hz (blue line: experimental Monte Carlo mean, dashed: experimental SEA(Tübitak Project Report, 112M836, 2015), red: FEM-Monte Carlo mean (Tübitak Project Report, 112M836, 2015), dotted: analytical SEA (Tübitak Project Report, 112M836, 2015))



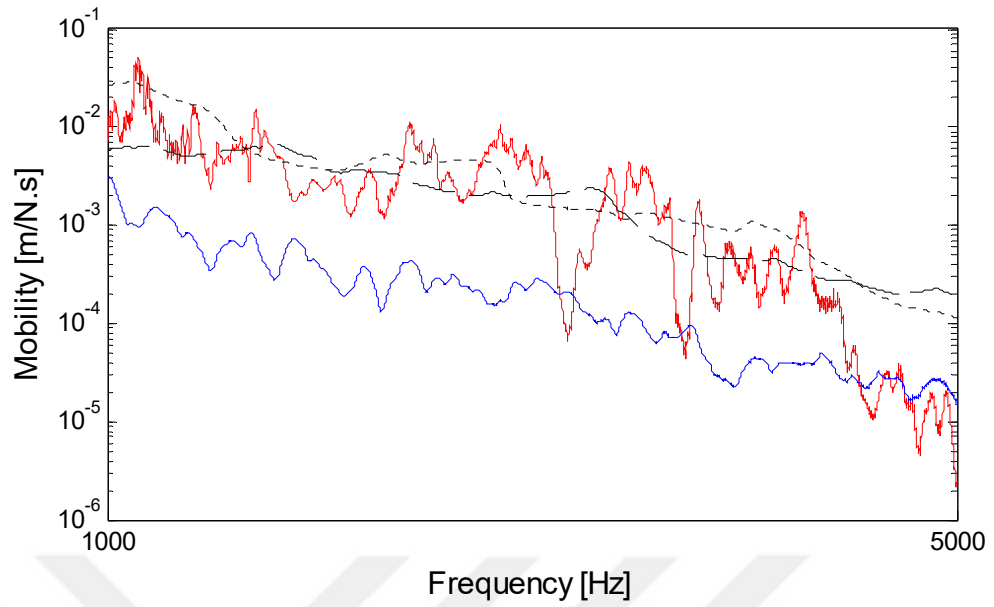
b)

Figure 5.9 Response comparison of subsystem 1 in T-type structure a) 10-1000 Hz, b) 1000-5000 Hz (blue line: experimental Monte Carlo mean, dashed: experimental SEA (Tübitak Project Report, 112M836, 2015), red: FEM-Monte Carlo mean (Tübitak Project Report, 112M836, 2015), dotted: analytical SEA (Tübitak Project Report, 112M836, 2015)) (continued)



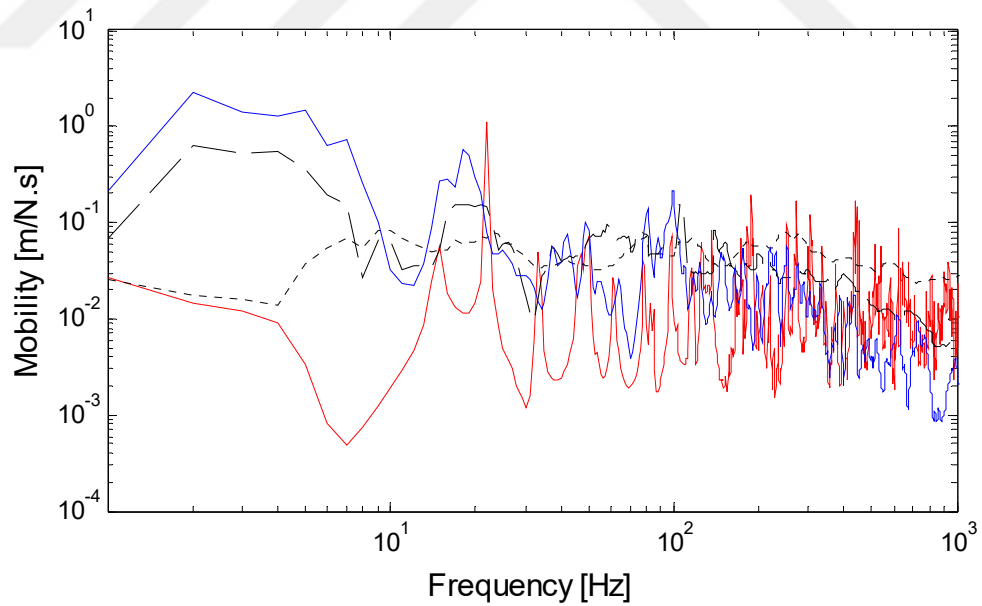
a)

Figure 5.10 Response comparison of subsystem 2 in T-type structure a) 10-1000 Hz, b) 1000-5000 Hz (blue line: experimental Monte Carlo mean, dashed: experimental SEA (Tübitak Project Report, 112M836, 2015), red: FEM-Monte Carlo mean (Tübitak Project Report, 112M836, 2015), dotted: analytical SEA (Tübitak Project Report, 112M836, 2015))



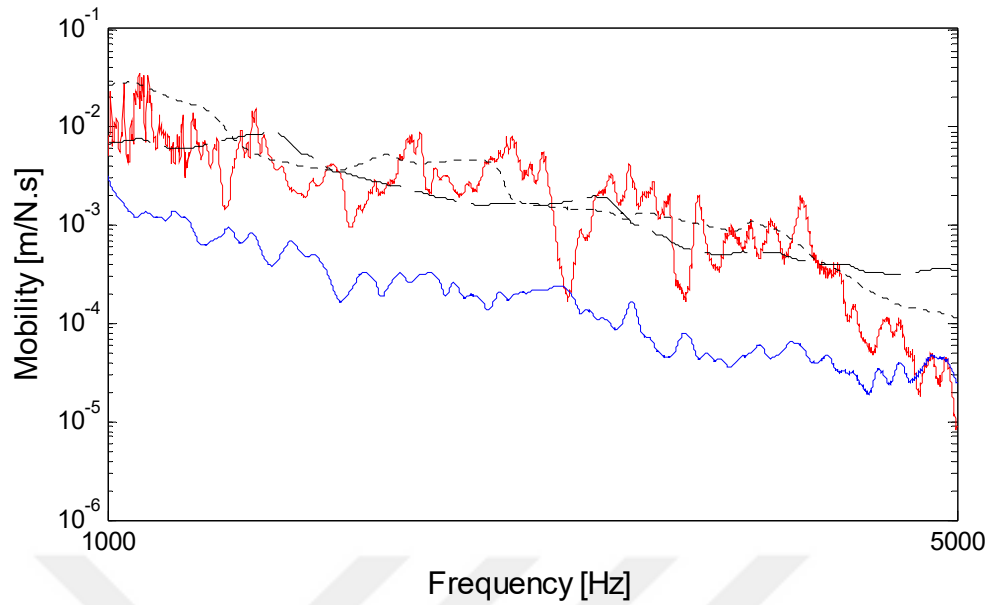
b)

Figure 5.10 Response comparison of subsystem 2 in T-type structure a) 10-1000 Hz, b) 1000-5000 Hz (blue line: experimental Monte Carlo mean, dashed: experimental SEA (Tübitak Project Report, 112M836, 2015), red: FEM-Monte Carlo mean (Tübitak Project Report, 112M836, 2015), dotted: analytical SEA (Tübitak Project Report, 112M836, 2015)) (continued)



a)

Figure 5.11 Response comparison of subsystem 3 in T-type structure a) 10-1000 Hz, b) 1000-5000 Hz (blue line: experimental Monte Carlo mean, dashed: experimental SEA (Tübitak Project Report, 112M836, 2015), red: FEM-Monte Carlo mean (Tübitak Project Report, 112M836, 2015), dotted: analytical SEA (Tübitak Project Report, 112M836, 2015))



b)

Figure 5.11 Response comparison of subsystem 3 in T-type structure a) 10-1000 Hz, b) 1000-5000 Hz (blue line: experimental Monte Carlo mean, dashed: experimental SEA (Tübitak Project Report, 112M836, 2015), red: FEM-Monte Carlo mean (Tübitak Project Report, 112M836, 2015), dotted: analytical SEA (Tübitak Project Report, 112M836, 2015)) (continued)

As seen in Figures 5.9-5.11 FEM-Monte Carlo responses are diverged from experimental results soon after 1000 Hz. As it is noted in the evaluation of Figure 5.8, this situation can be caused due to the fact that exciter could not sufficiently provoke the system after 1000 Hz properly. Besides that, SEA results converges FEM-Monte Carlo results at high frequency region as expected.

5.3 Uncertainty Analysis of Stiffened Plate

In this part of the study, a stiffened plate composed of one composite plate and two aluminum hollow beams was produced. Mechanical properties of the components are given in Table 5.2. Vibration velocity responses of each structure were predicted by SEA, FEM-Monte Carlo and experimental Monte Carlo simulation. Here the excitation force is applied as 1N for each method.

Table 5.2 Mechanical properties of the plate and beam

Property	Plate	Beam
Density [kg / m^3]	1771.21	2700
Modulus of Elasticity [MPa]	E_x : 21.30	69000
	E_y : 21.10	
Poisson Ratio	ν_{xy} : 0.161	0.33
External Dimensions [m x m x m]	1 x 1 x 2.2e-3	1 x 50e-3 x 50e-3
Internal Dimensions [m x m x m]	---	1 x 46e-3 x 46e-3
Structural Damping (η)	0.0286	0.0168

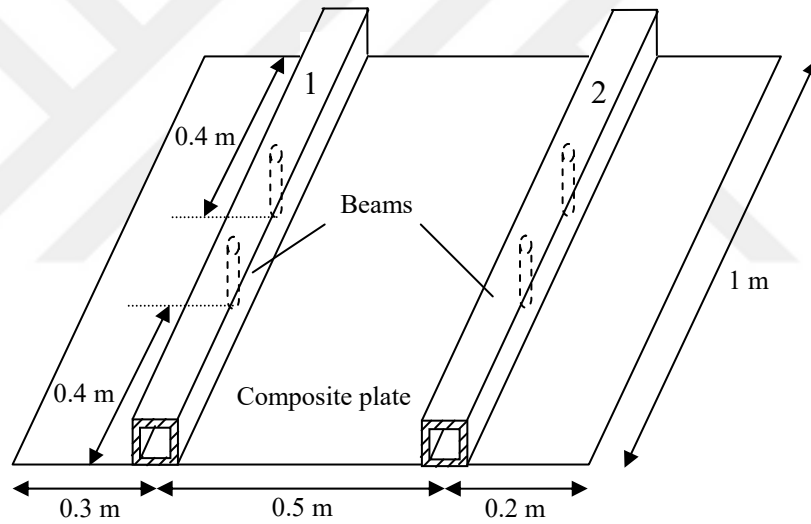


Figure 5.12 Stiffened plate

5.3.1 MOF values and High Frequency Thresholds

High frequency thresholds were approximately determined through Modal Overlap Factor (MOF) (Figure 5.13).

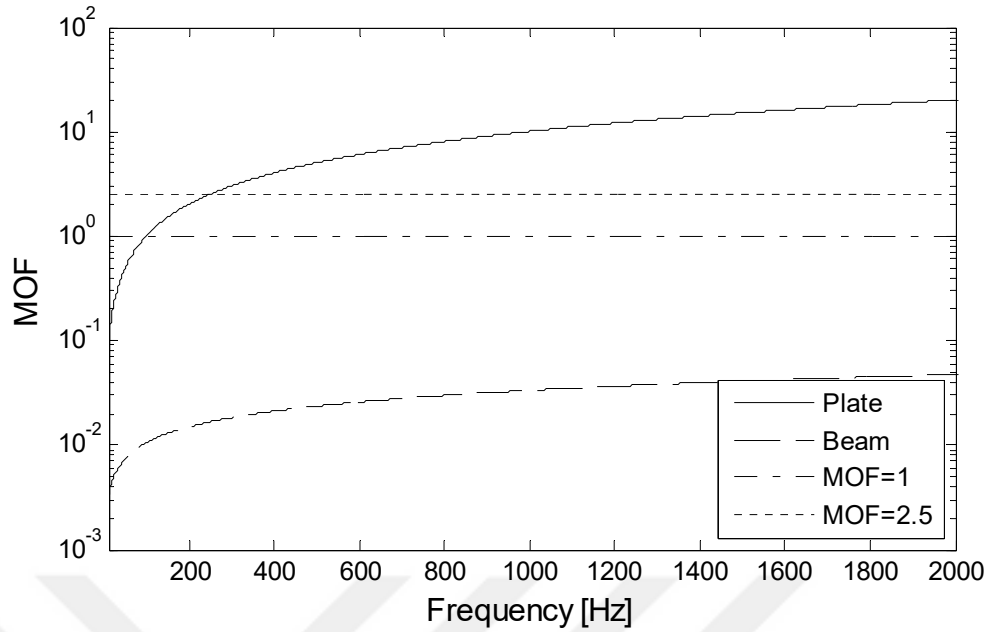


Figure 5.13 MOF values of structures and high frequency thresholds

As shown in Figure 5.13, high frequency threshold of the plate is 250 Hz at which the MOF is 2.5. However, the frequency range of the study could not reach the high frequency threshold for the beam. In this context, high frequency threshold was defined as 250 Hz for the stiffened plate.

5.3.2 *Vibration Velocity Response of Uncertain Stiffened Plate*

In experimental setup, stiffening beams were bolted to the plate as shown in Figure 5.14. This connection maintains a point connection for the structure. Experimental uncertainty simulation was implemented only to the plate during the analysis through adding small masses. Additional mass is 5% of the total mass of the plate. This additional mass was implemented to the structure by using 30 small lumped masses.

During the experiments masses were attached randomly to a hundred predefined points. The randomized spatial distribution of the added masses was generated via computer in advance. Accordingly, 20 distributions were generated and these distributions are presented in Table 5.3. The distribution was repeated for two

different excitation points. In each distribution, added masses were attached to the same points as indicated as light blue points in Table 5.3.

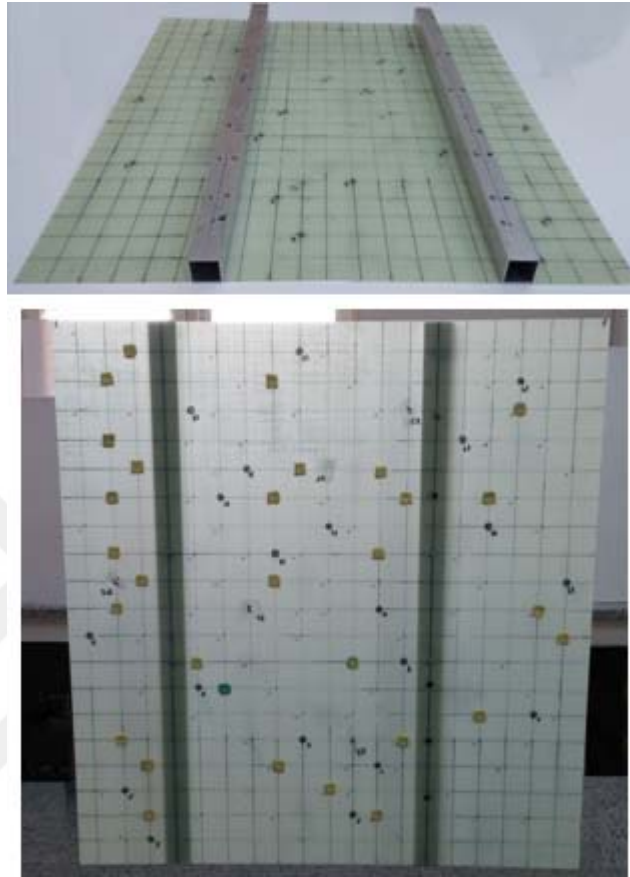
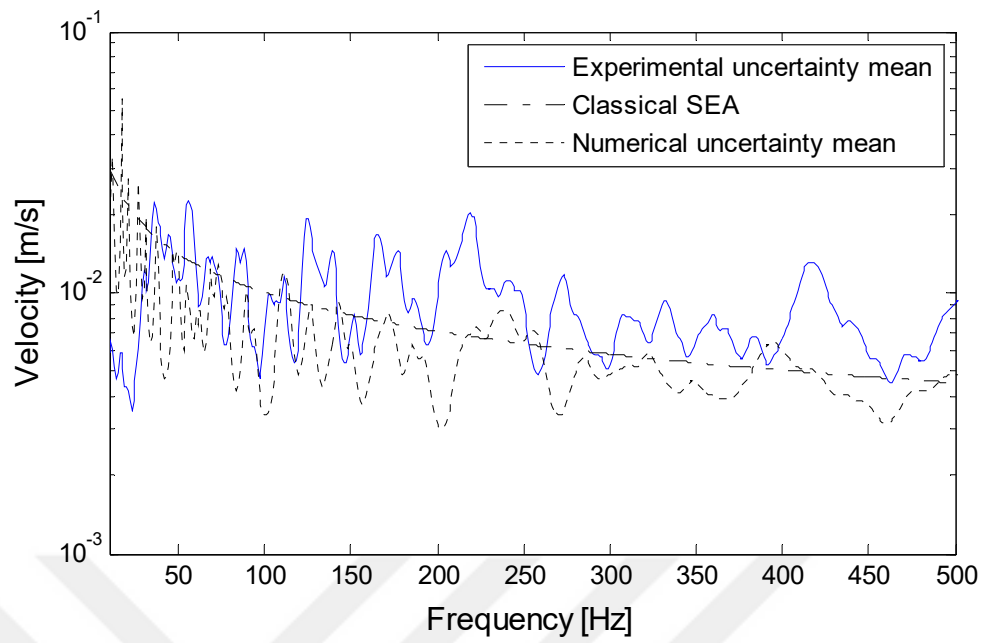


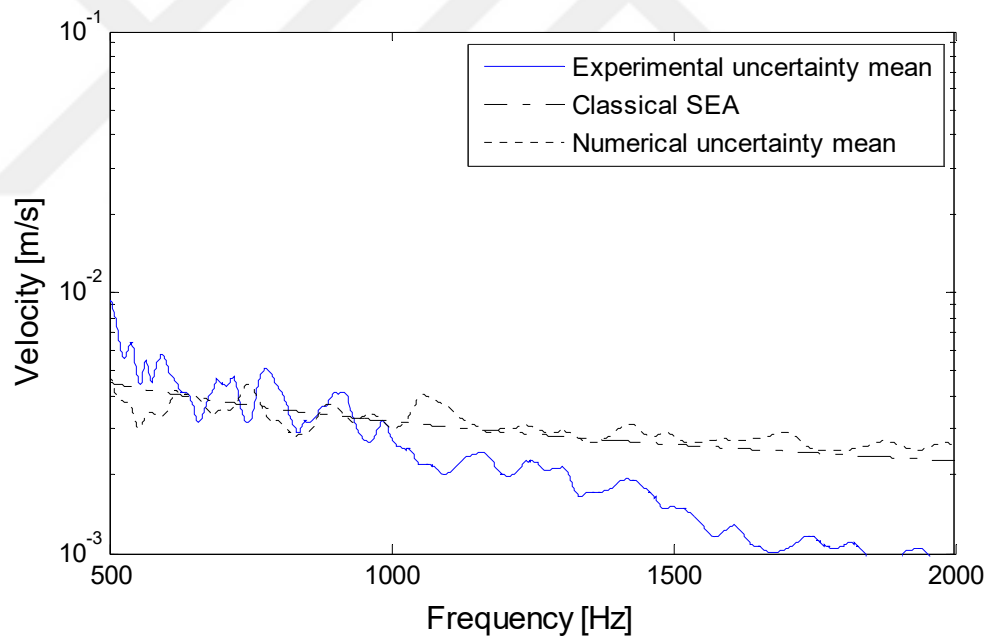
Figure 5.14 Stiffened plate and added mass distribution sample

Table 5.3 Experimental uncertainty distribution

Distribution number	Positions on the plate																													
1	7	10	13	19	20	23	25	27	34	37	39	40	45	50	54	56	58	62	68	69	71	73	75	76	78	83	84	93	95	100
2	2	4	5	6	7	9	13	24	26	30	34	36	40	47	48	52	53	58	65	67	69	74	75	79	81	83	85	87	89	99
3	1	10	12	16	21	22	23	24	27	28	29	30	31	37	39	40	41	46	48	58	59	61	64	65	66	81	95	96	97	100
4	5	8	14	18	21	23	28	31	33	45	48	49	54	59	60	62	63	64	65	77	79	80	83	87	88	92	95	98	99	100
5	2	3	9	14	15	16	19	21	26	35	37	42	43	52	53	54	56	57	59	63	66	69	70	76	79	80	86	93	94	95
6	4	7	8	9	10	12	14	18	31	37	40	47	49	51	53	55	59	63	65	68	71	72	83	85	91	92	93	96	97	99
7	1	2	3	7	12	14	21	26	28	31	32	38	39	44	45	47	49	53	62	67	68	71	72	73	76	81	87	92	94	98
8	2	10	11	17	21	22	27	28	35	41	47	50	51	52	53	57	66	68	70	74	76	77	80	81	85	86	89	95	97	98
9	2	3	6	10	11	17	18	22	24	25	28	31	33	35	43	45	46	47	48	53	59	60	61	62	71	81	84	87	88	98
10	1	5	6	7	10	12	15	17	18	21	25	26	31	40	47	51	53	58	62	63	64	73	78	84	85	89	90	92	94	99
11	4	5	6	7	9	12	14	16	19	29	44	45	49	55	56	60	63	66	69	72	74	77	78	79	81	84	85	87	93	96
12	3	6	10	16	17	22	24	27	33	46	47	50	51	62	71	73	74	78	81	86	87	88	90	91	93	94	95	96	99	100
13	2	3	12	13	14	16	31	34	35	46	48	52	53	57	58	61	64	66	70	72	76	77	81	83	84	85	87	93	99	100
14	4	7	11	14	15	17	21	33	37	39	41	42	46	47	52	55	61	62	68	70	71	76	79	81	84	85	90	93	97	100
15	2	3	14	20	22	26	28	29	30	44	45	48	49	52	65	67	71	72	74	78	79	80	83	88	90	91	92	97	99	100
16	2	4	6	7	14	20	24	25	28	37	39	42	45	47	48	50	51	52	54	56	58	59	60	65	67	77	80	89	91	96
17	3	6	7	8	13	16	18	27	28	30	33	34	36	38	41	45	47	50	51	53	54	56	59	79	81	82	86	91	92	94
18	7	8	12	13	17	20	21	22	25	26	27	29	33	37	38	44	55	58	62	63	67	71	73	74	75	76	80	83	89	90
19	1	14	19	22	25	29	34	39	41	42	44	49	51	52	55	61	64	67	69	76	80	81	83	84	85	88	90	91	92	93
20	2	6	7	9	14	16	17	19	20	23	29	31	34	38	42	46	52	59	61	69	72	82	85	87	88	89	92	93	96	99

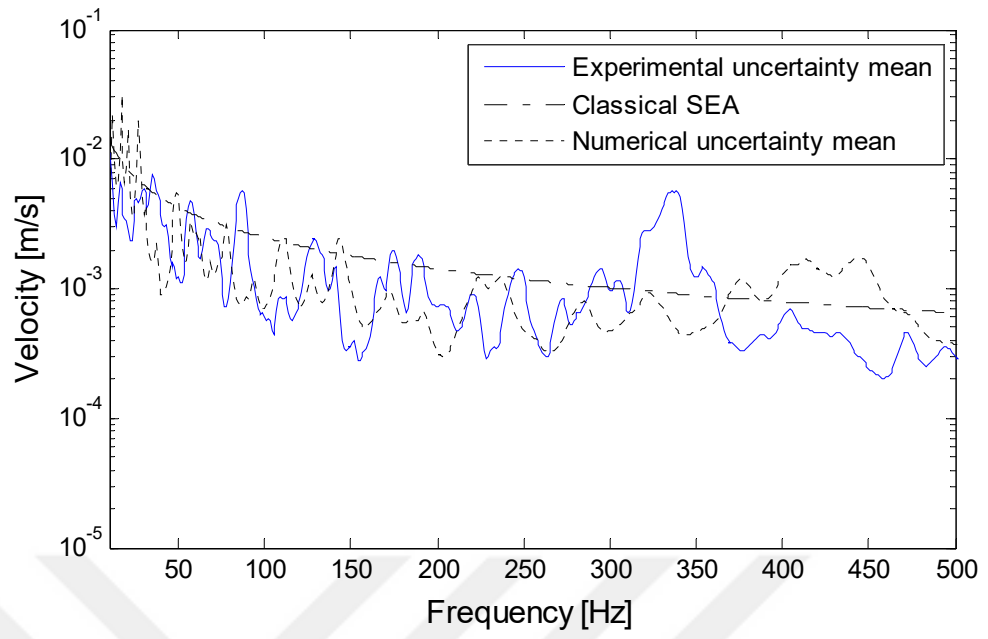


a)

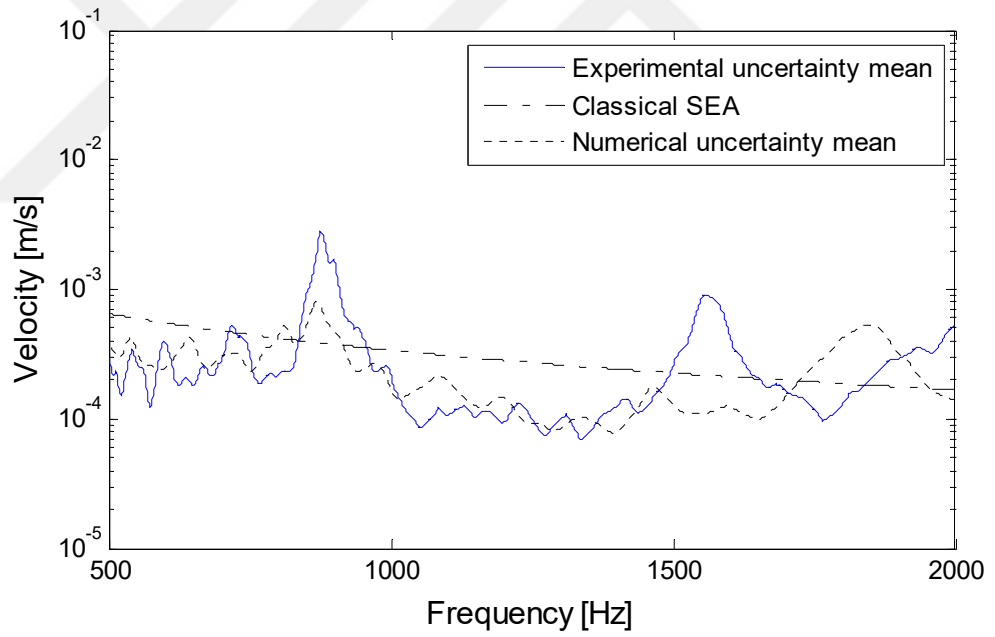


b)

Figure 5.15 Frequency response function of the plate a) 10-500 Hz, b) 500-5000 Hz

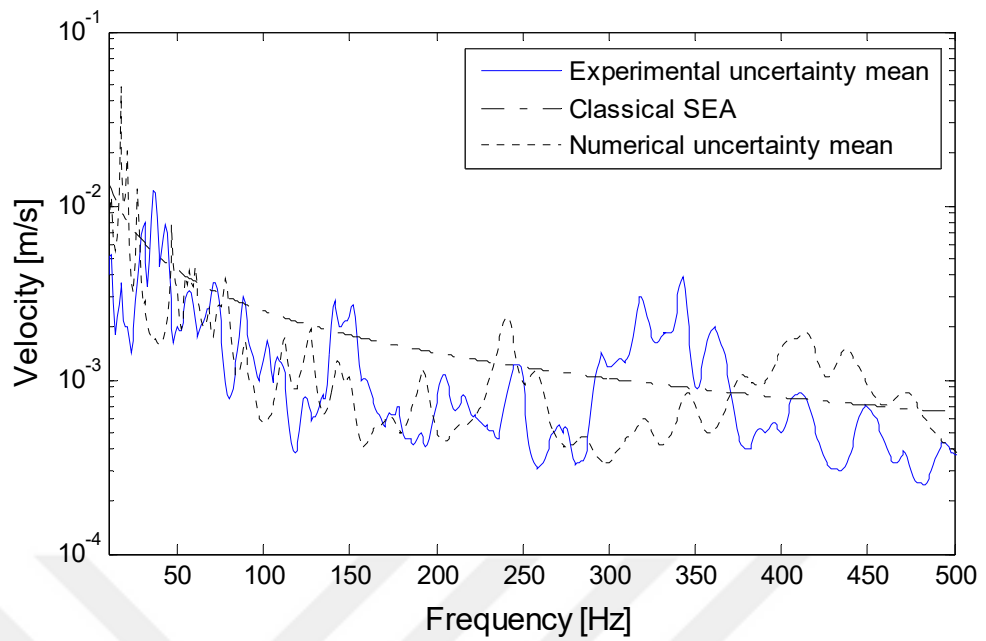


a)

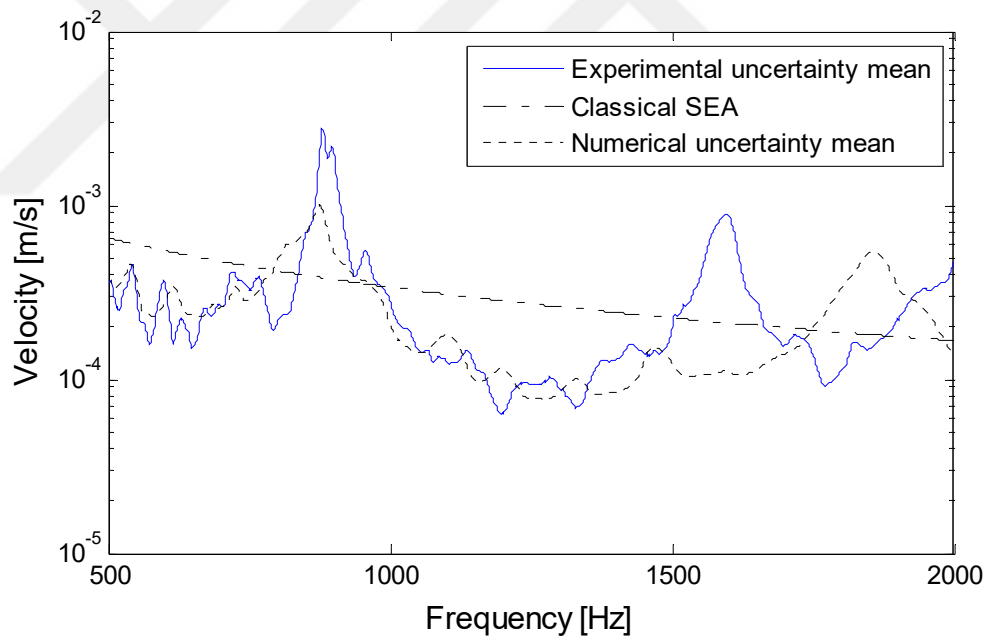


b)

Figure 5.16 Frequency response function of the 1st beam a) 10-500 Hz, b) 500-5000 Hz



a)



b)

Figure 5.17 Frequency response function of the 2nd beam a) 10-500 Hz, b) 500-5000 Hz

Here, in Figures 5.15-5.17 experimental results show the similar levels with the numerical results, however, for very high frequencies, after 1000Hz, it does not accurately predict the response. It can be caused by the insufficient number of measurement points. Since 250 Hz is approximately defined as the high frequency

threshold. Therefore, going beyond 250Hz, namely 1000Hz can be regarded as sufficient for such an analysis.

The discrepancies between experimental and numerical results, although their levels are seen as similar in certain areas, may be caused by improper application of practical uncertainty via adding small masses.

5.4 Uncertainty Analysis of Structural-Acoustic System: Cabinet

In this part of the study, a chassis was produced by using aluminum beams; these beams constitute a frame for the cabinet as shown in Figure 5.18a. Beams were bolted to each other thus it maintains point connection. Plates were glued only to the beams by epoxy resin (Figure 5.18). This attachment implies linear connection between beams and plates. Also the enclosed cabinet includes an acoustic cavity of air. This cavity interacts with the structure by the surfaces of the plates; through this the cavity is coupled to the structure providing area connection. The dimensions of the cabinet are shown in Figure 5.19.

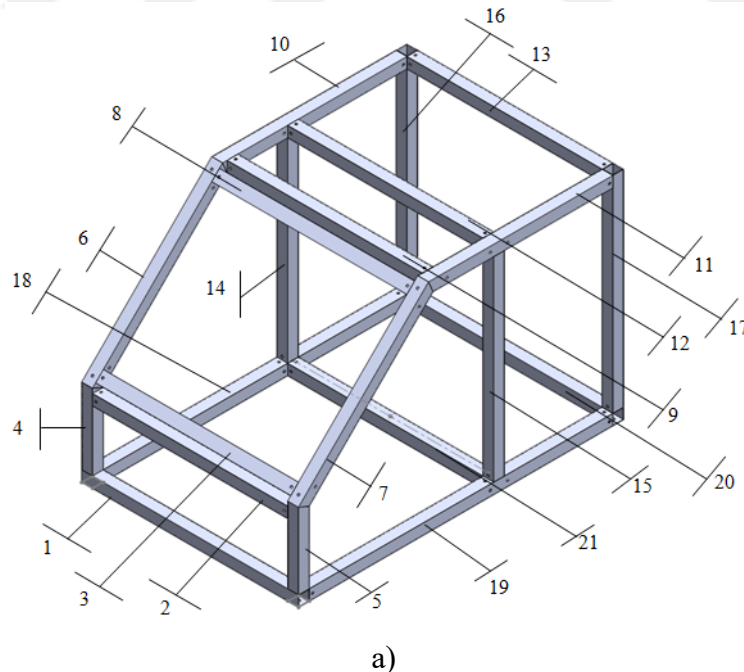
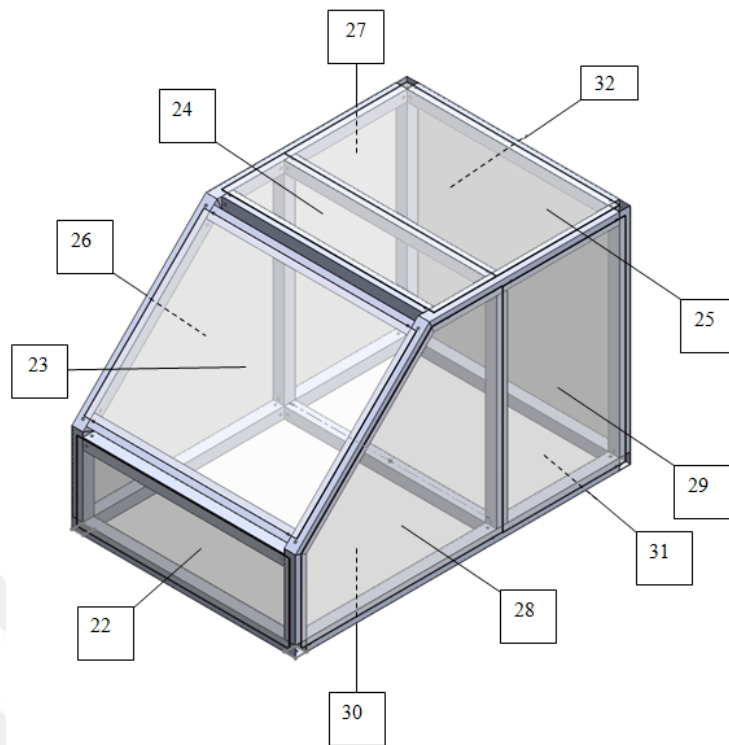


Figure 5.18 Design of the cabinet a) chassis, b) chassis + plates



b)

Figure 5.18 Design of the cabinet a) chassis, b) chassis + plates (continued)

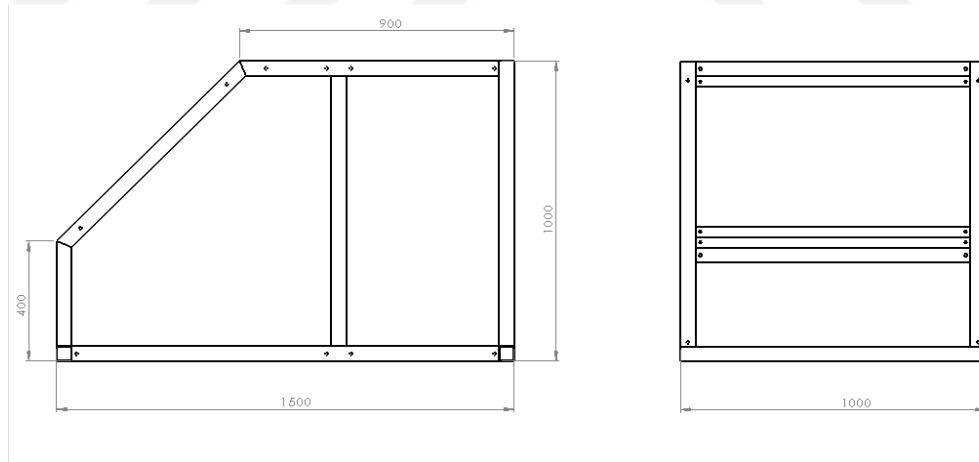


Figure 5.19 Dimensions of the cabinet design

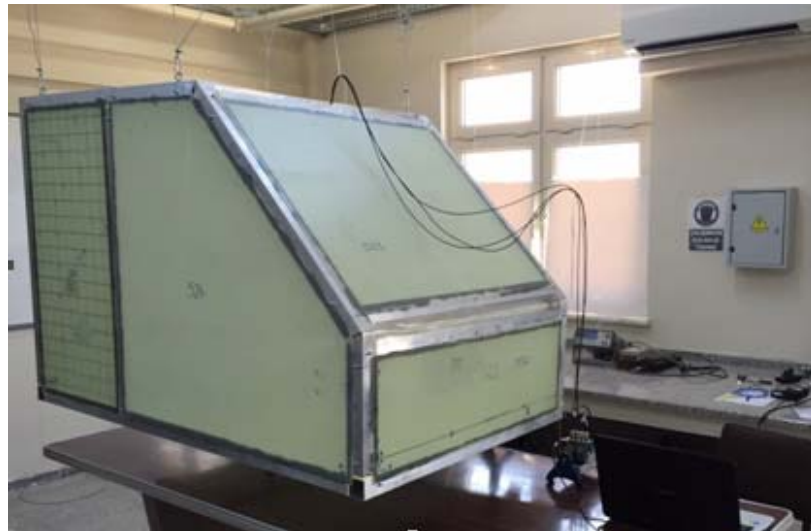
The total length of beams and total area of plates are given in Table 5.4.

Table 5.4 Total mass of beam and plate used to construct the cabinet model

	Total amount of use	Unit dimension mass	Total mass
50 x 50 x 2mm Aluminum hollow beam	21 m	1,075 kg/m	22,575 kg
8 layered composite plate	5,82 m ²	3,89 kg/ m ²	22,639 kg
		Total	45,214 kg

5.4.1 Manufacturing of the Cabinet

Here, manufactured cabinet is shown in Figure 5.20a. Inside the cabinet 30x90 cm² glass wool was placed to provide cabin sound absorption due to inner materials as shown in Figure 5.20b. For the constitution of excitation, a vibration motor with a constant frequency of 50 Hz was connected to the structure, as seen in Figure 5.20b.



a)

Figure 5.20 Manufactured cabinet model a) cabinet, b) position of vibration motor and damping material



b)

Figure 5.20 Manufactured cabinet model a) cabinet, b) position of vibration motor and damping material (continued)

Beside this an SEA model for the cabinet was constructed in the project and given in Figure 5.21.

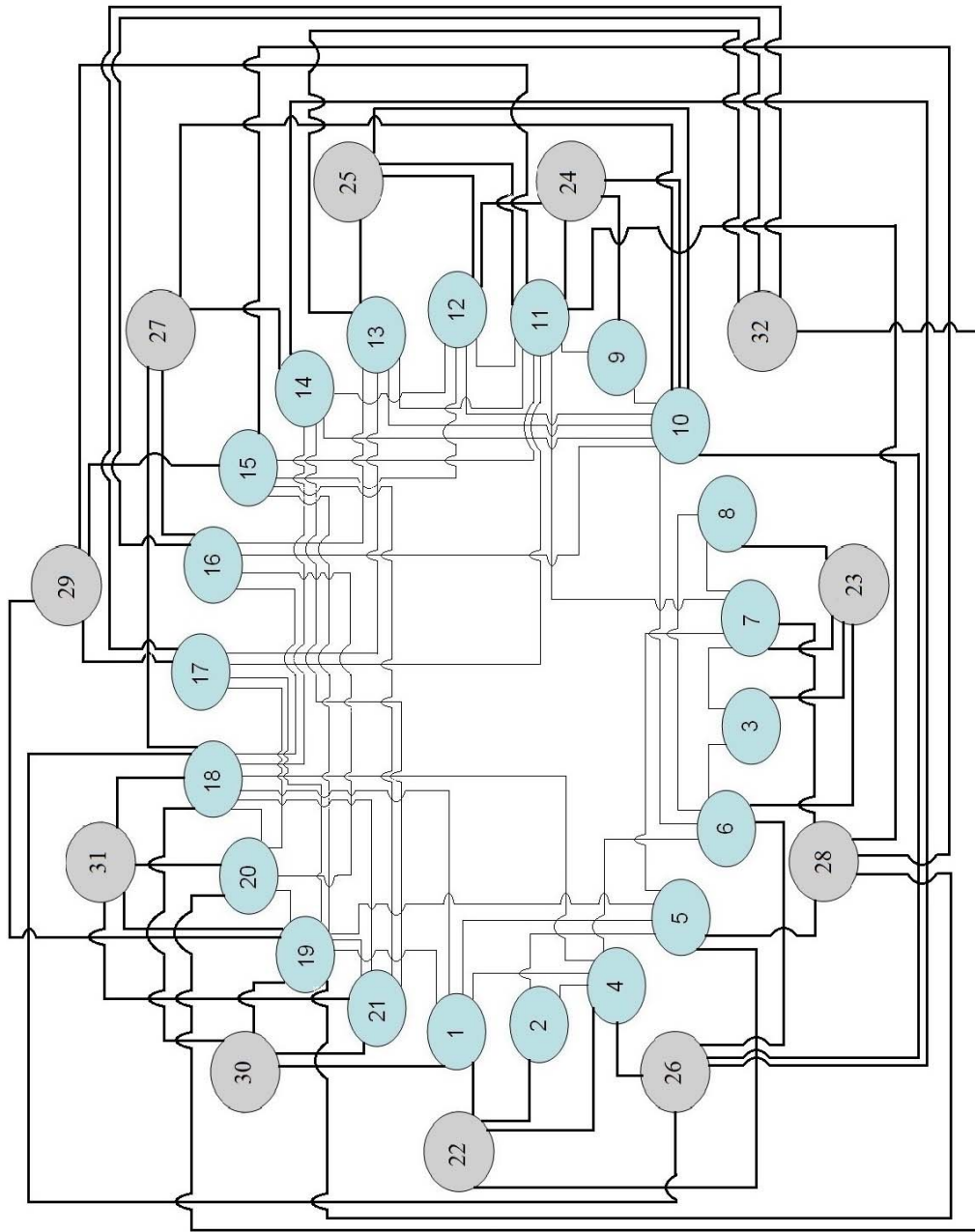


Figure 5.21 Structural SEA model of the cabinet SEA (Tübitak Project Report, 112M836, 2015)

5.4.2 Free Vibration Analysis of the Cabinet

In the supported project, numerical free vibration analysis was performed for four different cases; 1-Chassis, 2-Chassis+plate (without cavity), 3-Only acoustical cavity, 4-Entire system (Cabinet). First 30 natural frequencies were obtained and the results are tabulated in Table 5.5.

Since structural analyses were performed for free boundary condition, first 6 frequencies calculated as zero, as expected. The natural frequencies of the chassis + plate (Case 2) are obtained as higher than those of cabinet. Therefore it can be said that acoustical cavity shift the entire system to lower frequencies because the cavity creates a viscous damping effect to the system.

Table 5.5 Natural frequencies of the parts of the structure (Tübitak Project Report, 112M836, 2015)

	Chassis	Chassis + Plates	Acoustical cavity	Cabinet		Chassis	Chassis + Plates	Acoustical cavity	Cabinet
1	0,0000	0,0000	0,0000	0,0000	22	231,298	44,9699	434,1795	33,4913
2	0,0000	0,0000	125,0444	0,0001	23	242,902	45,5731	443,3845	33,9806
3	0,0002	0,0000	179,0704	0,0001	24	246,645	46,0864	451,3092	34,4097
4	0,0003	0,0000	185,7045	0,0002	25	255,153	46,1296	470,2514	36,4234
5	0,0007	0,0000	218,5245	0,0002	26	262,191	46,8787	478,3228	38,1055
6	0,0011	0,0003	222,0511	0,0000	27	264,036	49,2242	485,7900	38,5899
7	65,2624	15,3739	258,1917	9,3388	28	268,112	54,4583	504,7224	39,9650
8	76,4682	17,1512	272,0195	11,7591	29	270,514	56,6011	511,4808	40,7159
9	84,7680	17,4088	285,5275	13,2487	30	287,075	57,1375	512,3602	41,0497
10	86,2334	17,9347	325,3568	14,7012					
11	95,6441	22,0042	326,0144	15,5419					
12	116,8790	25,3502	358,8563	15,7434					
13	120,3191	27,4662	363,6114	17,1652					
14	143,3988	34,1980	371,8395	17,4309					
15	155,0860	34,7005	377,2050	18,7528					
16	167,5094	40,9535	380,2919	22,0379					
17	174,6696	42,7070	404,5984	25,9705					
18	201,4588	44,1960	405,0293	27,1989					
19	209,7874	44,2365	405,8328	28,3557					
20	210,1449	44,5766	418,1030	30,5502					
21	211,0948	44,7539	422,7278	31,0042					

5.4.3 Frequency Response Function of the Cabinet

Here, a beam on the floor of the cabinet (Subsystem 21) was excited by a vibration motor as shown in Figure 5.20b. Frequency response functions were obtained due to this excitation. Experimental results were compared with numerical and SEA results which are obtained from the project. Excitation characteristic of the vibration motor were revealed from the measurement as given in Figure 5.22, and fed to the numerical model. Here, excitation force was calculated by the multiplication of the acceleration and mass of the beam and connected vibration motor.

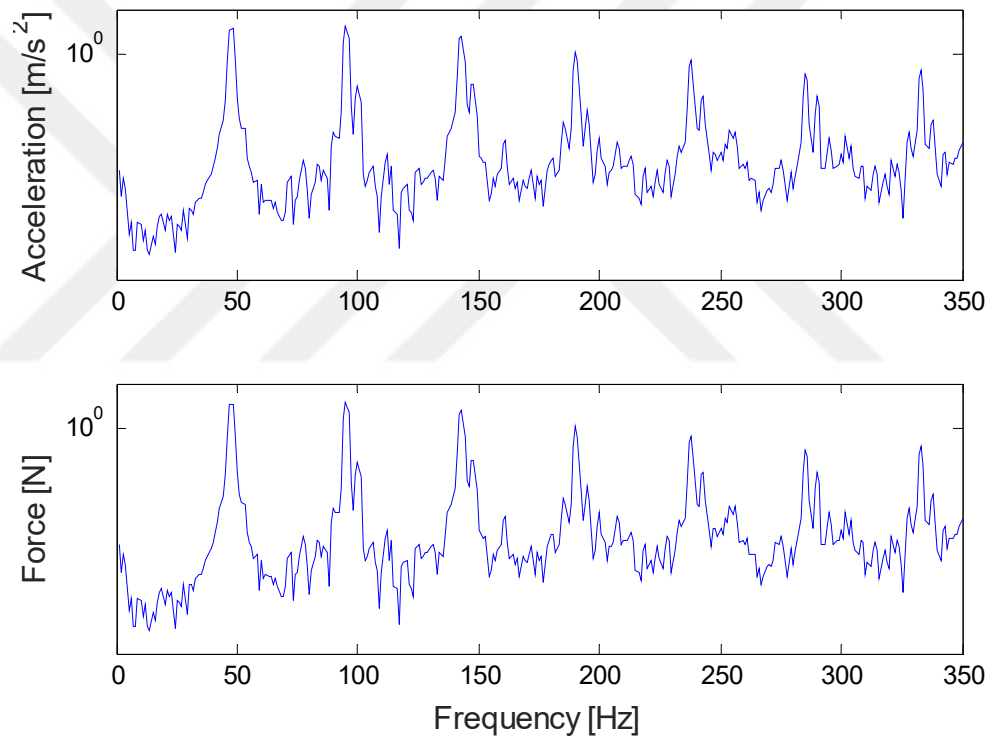


Figure 5.22 FRF of the excitation implemented to the cabinet a) acceleration, b) force

5.4.4 Uncertainty Analysis of the Cabinet

After the determination of the excitation characteristics, uncertainty characteristics of the system were investigated. Mass of the left side plate (Subsystem 28) was selected as the uncertainty parameter. Measurements were performed for 10 mass distributions. In each distribution, 10 fixed points on the plate

and 3 points in acoustical cavity are utilized. Therefore, 100 acceleration, and 30 sound pressure data are used for average responses. Experimental setup of this uncertainty measurement can be seen in Figure 5.23. Results of these analyses are presented for acceleration response in Figure 5.24 and for sound pressure level (SPL) in Figure 5.25.

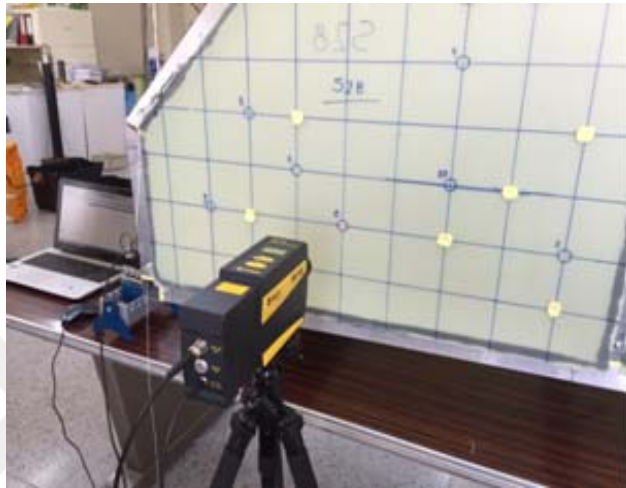


Figure 5.23 Experimental uncertainty setup of the cabinet

As seen in Figure 5.24 and 5.25 response functions are in harmony. It leads to numerical and analytical models are accurately constructed. As the frequency increases, numerical and experimental results are getting much closer in this considered frequency of interest (0-350 Hz). This can be because of decreasing the effect of boundary conditions in low frequencies.

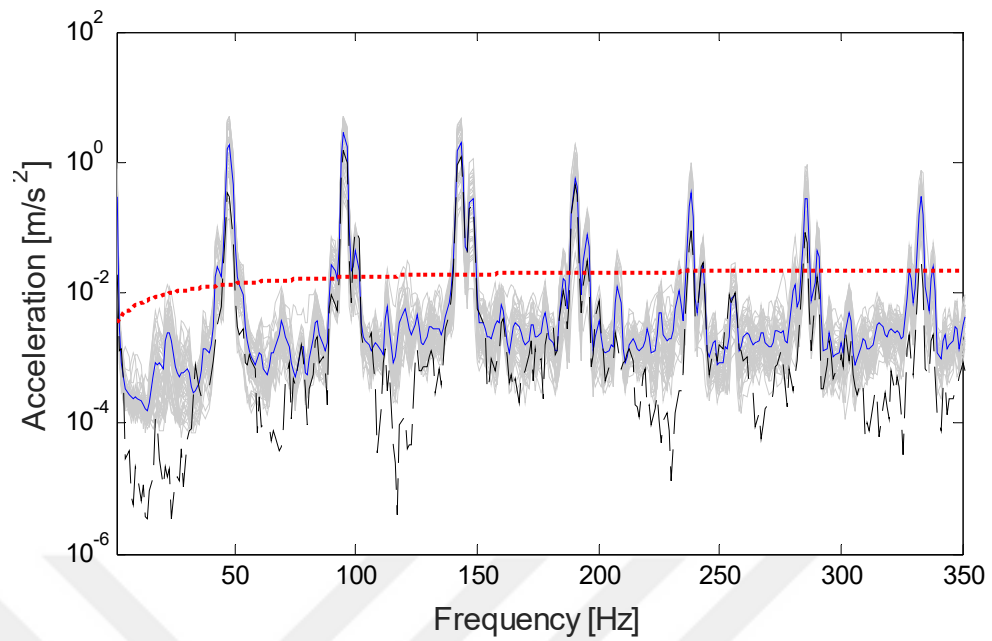


Figure 5.24 Acceleration responses of the uncertain plate (28th subsystem) (grey: uncertainty results, blue line: experimental uncertainty mean, black dashed: FEM results (Tübitak Project Report, 112M836, 2015), red dotted: analytical SEA (Tübitak Project Report, 112M836, 2015))

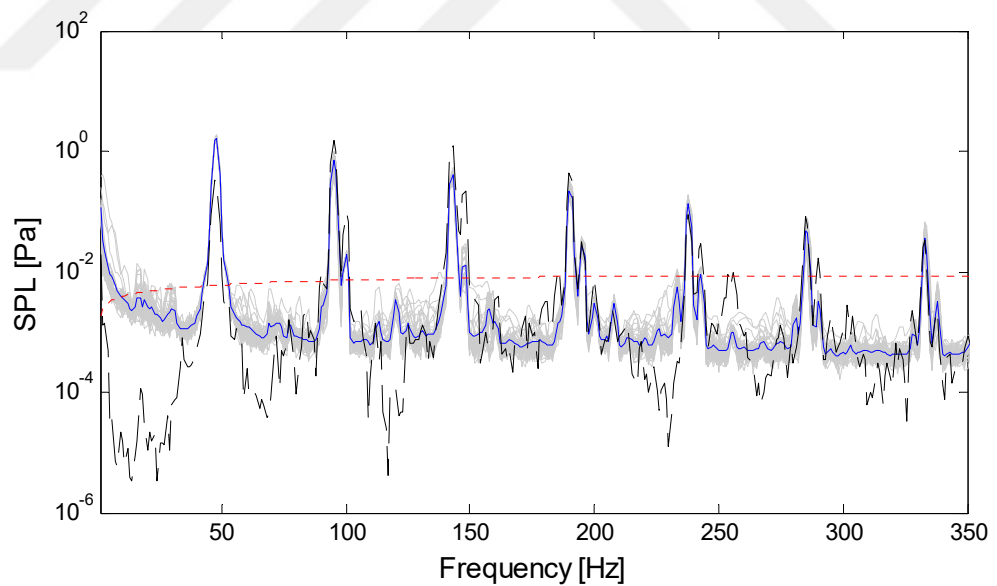


Figure 5.25 Sound pressure levels of the acoustical cavity (grey: uncertainty results, blue line: experimental uncertainty mean, black dashed: FEM results (Tübitak Project Report, 112M836, 2015), red dotted: analytical SEA (Tübitak Project Report, 112M836, 2015))

Figure 5.24 and 5.25 showed that numerical and experimental predictions very well converge. This leads that, application of small masses to simulate uncertainties can be reliably used in complex structural acoustic systems.



CHAPTER SIX CONCLUSION

Increasing application of composite materials and structures in engineering industries for their preferred advantages leads a shifting in vibro-acoustic response through mid and high frequency region due to their light weight. In order to achieve accurate results in these regions with conventional methods require high solution time and memory usage, which makes them inefficient. Notwithstanding, some statistical energy based methods can predict accurate results solely in high frequency region. As a consequence of that situation an unclear region, mid frequency region constitutes.

In the study, various types of composite structures made of plates and isotropic beams were used. The structures were connected to each other by point and line connections via bolts and epoxy based adhesives, respectively.

Analyses started with an experimental modal analysis for the following structures; an aluminum hollow beam, a single composite plate, T-Shaped composite plate. Experimental results were utilized in the verification of numerical predictions.

Secondly, determination of statistical energy analysis parameters such as coupling and damping loss factors of the structures were successfully made via experimental power injection method (PIM) for the following structures; an aluminum hollow beam, a single composite plate, I-, L- and T-type composite plate structures. These factors were used in statistical energy analysis (SEA) method in order to predict mid and high frequency responses.

In the final part of the study, experimental uncertainty analysis based on numerical and experimental Monte Carlo analysis was considered for the following structures; A single composite plate, a T-type structure, a stiffened composite plate and a cabinet structure having acoustic volume.

All these studies with verifications in the thesis clearly showed that the experimental techniques used in this study can be reliably applied from simple to very complex structures. However, for higher frequencies, experimental techniques are not as accurate as it is in lower frequencies. Beside this, composite systems can be also treated by using these experimental techniques, especially having uncertain parameters.



REFERENCES

- Batou, A., Soize, C., & Audebert, S. (2015). Model identification in computational stochastic dynamics using experimental modal data. *Mechanical Systems and Signal Processing*, 50-51, 307-322.
- Bies, D.A., & Hamid, S. (1980). In situ determination of coupling loss factors by the power injection method. *Journal of Sound and Vibration*, 70, 187–204.
- Berthaut, J., Ichchou, M. N., & Jezequel, L. (2005). K-space identification of apparent structural behaviour. *Journal of Sound and Vibration*, 280, 1125-1131.
- Bloss, B.C., & Rao, M.D. (2005). Estimation of frequency-averaged loss factors by the power injection and the impulse response decay methods. *The Journal of the Acoustical Society of America*, 117, 240-249.
- Chierichetti, M., Grappasonni, C., Coppotelli, G., & McColl, C. (2014). A modal approach for dynamic response monitoring from experimental data. *Mechanical Systems and Signal Processing*, 48(1-2), 199-217.
- Cherif, R., Chazot, J. D., & Atalla, N. (2015). Damping loss factor estimation of two-dimensional orthotropic structures from a displacement field measurement. *Journal of Sound and Vibration*, 356, 61-71.
- Clemente, P., Marulo, F., Lecce, L., & Bifulco, A. (1998). Experimental modal analysis of the Garigliano Cable-Stayed bridge. *Soil Dynamics and Earthquake Engineering*, 17, 485-493.
- Evans, M., & Swartz, T. (2000). *Approximating Integrals via Monte-Carlo and Deterministic Methods*. New York: Oxford University Press.

- Fahy, F.J. (1994). Statistical energy analysis: a critical overview. *Philosophical Transactions of the Royal Society A: Mathematical, Physical & Engineering Sciences*, 346, 431-447.
- Fahy, F. J., & Ruivo, H. M. (1997). Determination of statistical energy analysis loss factors by means of an input power modulation technique. *Journal of Sound and Vibration*, 203(5), 763-779.
- Fahy, F. J. (1998). An alternative to the SEA coupling loss factor: rationale and method for experimental determination. *Journal of Sound and Vibration*, 214, 261-267.
- He, J. & Fu, Z.F. (2001). *Modal analysis*. Oxford: Butterworth Heinemann.
- Hohenbichler, M., & Rackwitz, R. (1988). Improvement of second-order reliability estimates by importance sampling. *Journal of Engineering Mechanics*, 114, 2195–2199.
- Hooper, J., M., & Marco, J. (2015). Experimental modal analysis of lithium-ion pouch cells. *Journal of Power Sources*, 285, 247-259.
- Keane, A., & Price, W. (1997). *Statistical energy analysis*. Cambridge: Cambridge University Press.
- Lalor, N. (1997). The practical implementation of SEA. *IUTAM Symposium on SEA*, 257-268
- Langhe, K.D., & Sas, P. (1996). Statistical analysis of the power injection method. *The Journal of the Acoustical Society of America*, 100(1), 294-303.

- Langley, R. S., Bremner, P. (1998). A hybrid method for the vibration analysis of complex structural-acoustic systems. *The Journal of the Acoustical Society of America*, 105, 1657-1671
- Lewis, E.E., & Böhm, F. (1984). Monte Carlo simulation of markov unreliability methods. *Nuclear Engineering and Design*, 77, 49-62.
- Liang, X., Jun, G., J., & Jing, J., J. (2001). Experimental modal analysis of the HuMen Suspension Bridge. *Structural Engineering, Mechanics and Computation*, 1, 613-619.
- Lyon, R. H., & DeJong, R. G. (1998). *Statistical energy analysis (2nd ed.)*. Boston: RH Lyon Corp.
- Manik, D. N., (1988). A new method for determining coupling loss factors for SEA. *Journal of Sound and Vibration*. 211(3), 521-526.
- Maxit, L., & Guyader, J-L. (2009a). Estimation of SEA coupling loss factors using a dual formulation and FEM modal information, part I: Theory. *Journal of Sound and Vibration*, 239(5), 907-930.
- Maxit, L. & Guyader, J-L. (2009b). Estimation of SEA coupling loss factors using a dual formulation and FEM modal information, part II. Numerical applications. *Journal of Sound and Vibration*, 239(5), 931-948.
- McDaniel, J.G., & Dupont, P. (2000). A wave approach to estimating frequency-dependent damping under transient loading. *Journal of Sound and Vibration*, 231, 433-449
- Ming, R. (2005). An experimental comparison of the sea power injection method and the power coefficient method. *Journal of Sound and Vibration*, 282, 1009-1023.

- Oliveira, E., L., Maia, N., M., M., Marto, A., G., da Silva, R., G., A., Afonso, F., J., & Suleman, A. (2016). Modal characterization of composite flat plate models using piezoelectric transducers. *Mechanical Systems and Signal Processing*. DOI:10.1016/j.ymsp.2016.02.046 (In Press).
- Rabbiolo, G., Bernhard, R.J., & Milner, F.A. (2004). Definition of a high-frequency threshold for plates and acoustical spaces. *Journal of Sound and Vibration*, 277, 647–667.
- Rao, S.S., (1995). *Mechanical vibrations (3rd ed.)*. Reading: Addison-Wesley Publishing Company.
- Seçgin, A., Sarıgül, A. S. (2009). A novel scheme for the discrete prediction of high-frequency vibration response: discrete singular convolution–mode superposition approach. *Journal of Sound and Vibration*, 320, 1004-1022.
- Seçgin, A., (2013). Numerical determination of statistical energy analysis parameters of directly coupled composite plates using a modal based approach. *Journal of Sound and Vibration*, 332(2), 361-377.
- Seçgin, A., Güler, S., & Kara, M. (2015). Determinations of in-situ energy loss factors of point- connected composite plates. *Composites Part B: Engineering*. 87, 27-32.
- Seçgin, A., Kara, M., & Ozankan, A., (2015). A modal impedance technique for mid and high frequency analysis of uncertain stiffened composite plate. *Journal of Sound and Vibration*, 366, 396-406.
- Shorter, P.J., & Langley, R.S. (2005). Vibro-acoustic analysis of complex systems. *Journal of Sound and Vibration*, 288, 669–699.

- Steel, J. A., & Craik, R. J. M., (1994). Statistical energy analysis structure-borne sound transmission by finite element method. *Journal of Sound and Vibration*, 178(4), 553-561.
- Vanmaele, C., Vandepitte, D., & Desmet, W. (2007). An efficient wave based prediction technique for plate bending vibrations. *Computer Methods in Applied Mechanics and Engineering*, 196(33-34), 3178–3189.
- Vlahopoulos, N., & Zhao, X. (2001). An investigation of power flow in the midfrequency range for systems of co-linear beams based on a hybrid finite element formulation. *Journal of Sound and Vibration*, 243(3), 445–473.
- Whitney, J. M. (1987). *Structural Analysis of Laminated Anisotropic Plates*. Pennsylvania: Technomic Publishing Company Inc.
- Xu, L., & M., Guo, N. (2003). Modal testing and finite element modeling of subsystem in hard disk drive, *Mechanical Systems and Signal Processing*, 17(4), 747- 764.
- Zhang, P., Q., Tang, X., L., Shan, B., X., Brandon, J., A., & Kwan, A., S. (1998). Analytical and experimental modal analysis for operational validation and calibration of a miniature silicon sensor, *Journal of Sound and Vibration*, 214/1998(5), 903-913.
- Zhong, J., Zhong, S., & Zhang, Q. (2016). Two-dimensional optical coherence vibration tomography for low frequency vibration measurement and response-only modal analysis. *Mechanical Systems and Signal Processing*. DOI: 10.1016/j.ymssp.2016.02.027 (In Press).

APPENDIX A MODAL ANALYSIS TEST SETUP

Sensors:

- 3- Impact Hammer:
Model: PCB Piezotronics 086C03
Sensitivity: 2.416 mV/N
- 3- Accelerometer 1:
Model: PCB Piezotronics 352C33
Sensitivity: 101.6 mV/g
- 3- Accelerometer 2:
Model: PCB Piezotronics 352C33
Sensitivity: 103 mV/g

DAQ system:

- 1- Analog Input Card:
Model: National Instruments
NI9234
Input: 4 channel BNC
ADC resolution: 24 bits
- 2- DAQ Chassis:
Model: National Instruments
NI9174
Slots: 4 slots
Connection: USB

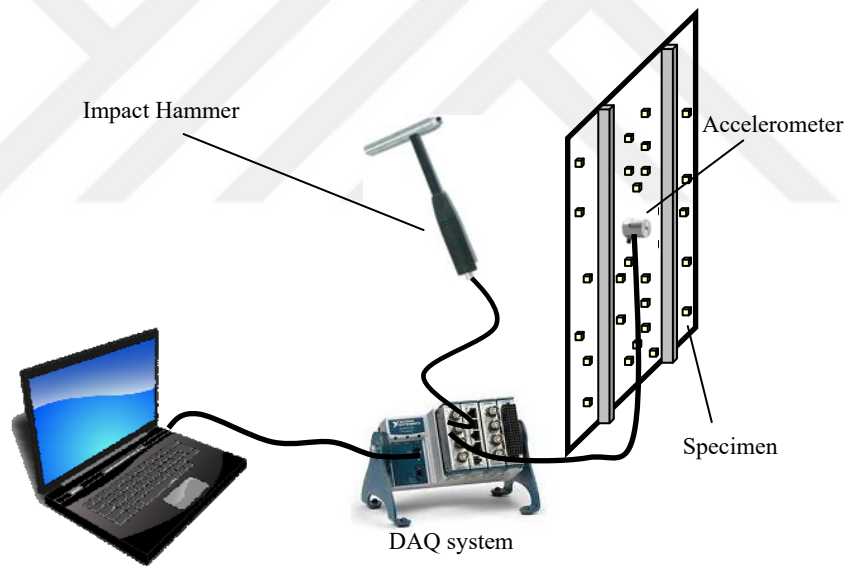


Figure A.1 Modal analysis system setup

APPENDIX B FREQUENCY RESPONSE ANALYSIS TEST SETUP

Sensors:

- 1- Impedance Head:
Model: PCB Piezotronics 288D01
Sensitivity Force: 22.18 mV/N
Sensitivity Acceleration: 98.3 mV/g
- 2- Accelerometer 1:
Model: PCB Piezotronics 352C33
Sensitivity: 101.6 mV/g
- 3- Accelerometer 2:
Model: PCB Piezotronics 352C33
Sensitivity: 103 mV/g

Excitation System:

- 1- Signal Generator:
Model: Agilent 33210A 10MHz
Function/Arbitrary Waveform
Generator
- 2- Power Amplifier:
Model: Brüel & Kjær Type 2706
Power Amplifier
- 3- Vibration Exciter:
Model: Brüel & Kjær Type 4809
Vibration Exciter

DAQ system:

- 1- Analog Input Card:
Model: National Instruments
NI9234
Input: 4 channel BNC
ADC resolution: 24 bits
- 2- DAQ Chassis:
Model: National Instruments
NI9174
Slots: 4 slots
Connection: USB

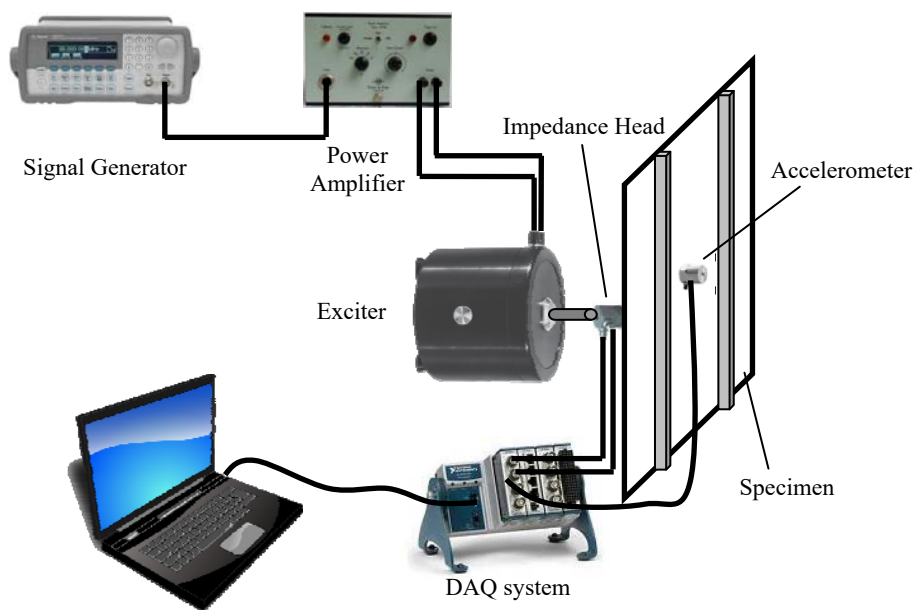


Figure B.1 Frequency response analysis system setup

APPENDIX C
UNCERTAINTY ANALYSIS SETUP

Sensors:

- 1- Laser Vibrometer:
Model: Polytec PDV 100
Sensitivity: 200 mV/mm/s, 40
mV/mm/s, 8 mV/mm/s
- 2- Microphone 1:
Model: G.R.A.S. 46BD ¼”
Pressure Microphone
Sensitivity: 1.99 mV/Pa
- 3- Microphone 2:
Model: G.R.A.S. 46BD ¼”
Pressure Microphone
Sensitivity: 1.98 mV/Pa
- 4- Microphone 3:
Model: G.R.A.S. 46BD ¼”
Pressure Microphone
Sensitivity: 1.53 mV/Pa
- 5- Accelerometer 1:
Model: PCB Piezotronics 352C33
Sensitivity: 101.6 mV/g
- 6- Accelerometer 2:
Model: PCB Piezotronics 352C33
Sensitivity: 103 mV/g

Excitation System:

- 1- Vibration Motor:
Model: Kem-P MV – 2M Vibration
Motor
Frequency: 3000 RPM (50 Hz)
Dynamic Force: 3.485 N
- 2- Signal Generator:
Model: Agilent 33210A 10MHz
Function/Arbitrary Waveform
Generator
- 3- Power Amplifier:
Model: Brüel & Kjær Type 2706
Power Amplifier
- 4- Vibration Exciter:
Model: Brüel & Kjær Type 4809
Vibration Exciter

DAQ system:

- 1- Analog Input Card:
Model: National Instruments
NI9234
Input: 4 channel BNC
ADC resolution: 24 bits
- 2- DAQ Chasis:
Model: National Instruments
NI9174
Slots: 4 slots
Connection: USB

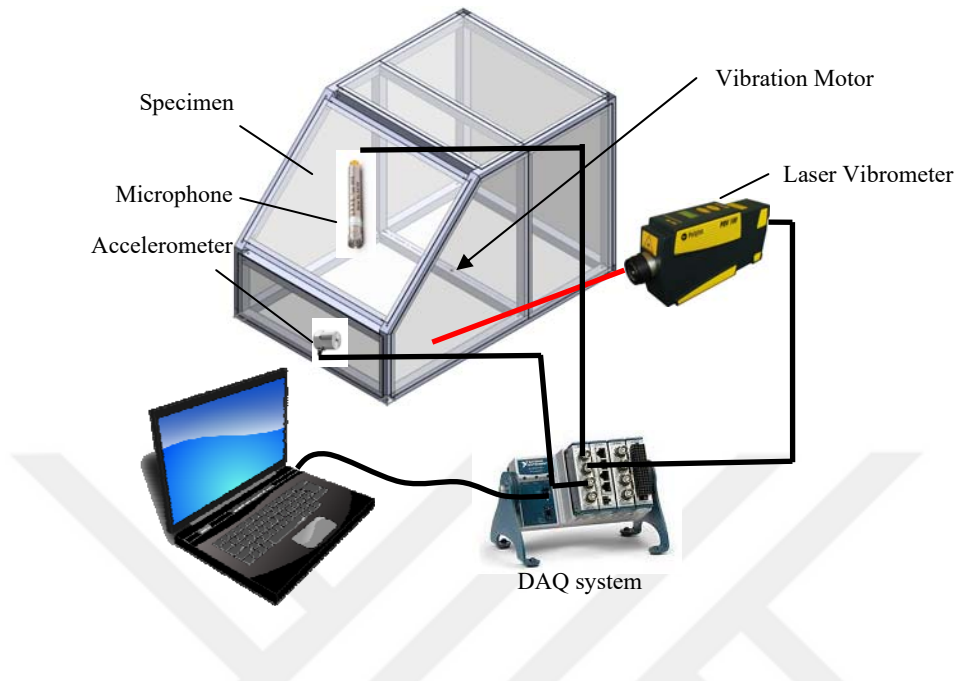


Figure C.1 Uncertainty analysis with vibration motor system setup

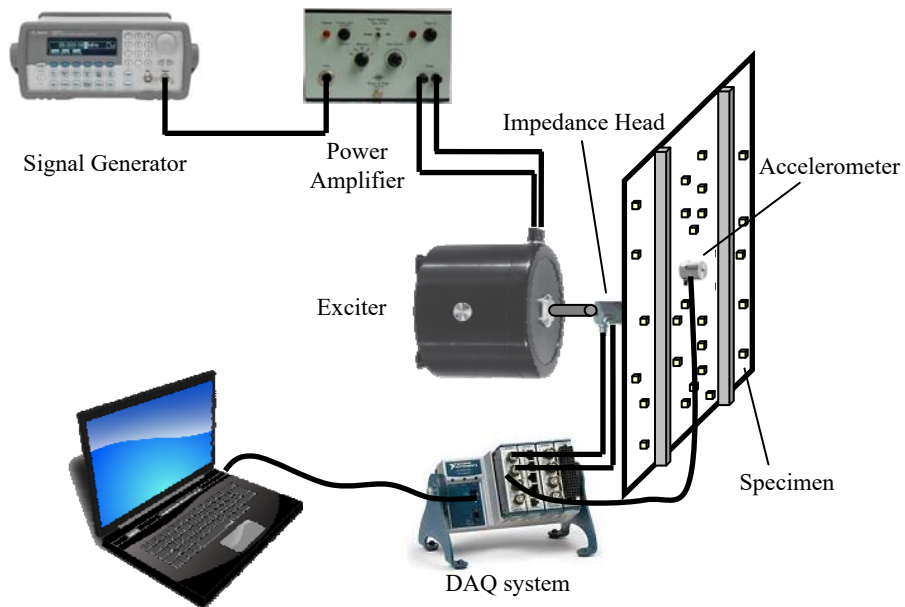


Figure C.2 Uncertainty analysis with vibration exciter system setup